HP-3

CR 160155

TUSKEGEE INSTITUTE

SCHOOL OF MECHANICAL ENGINEERING

TUSKEGEE INSTITUTE, ALABAMA

FOURTH ANNUAL REPORT: HEAT PIPE RADIATORS FOR SPACE

CONTRACT NO. NAS9-13844(6S)

BY

JOHN P. SELLERS

SPONSORED BY

ENVIRONMENTAL AND THERMAL SYSTEMS SECTION

MANNED SPACECRAFT CENTER

NATIONAL AERONAUTICS AND SPACE ADMINISTRATION

HOUSTON, TEXAS

SEPTEMBER, 1977

FOURTH ANNUAL REPORT: HEAT PIPE RADIATORS FOR SPACE

BY

J. P. SELLERS

Tuskegee Institute

Contract NAS9-13844 (Mod. 6S)

September, 1977

FORWARD

This report was prepared for Johnson Space Center of the National Aeronautics and Space Administration. The work was performed under Contract NAS9-13844 with Mr. W. Ellis, Mr. B. French and Dr. L. Kuznetz providing NASA direction.

The work was performed from September 1975 to August 1976. The author would like to acknowledge the assistance of Mr. Ting-Chang Huang, and to express his appreciation to Tuskegee Institute for granting permission to undertake the task.

ABSTRACT

Analysis of new data obtained by Johnson Space Center on a heat-pipe radiator system tested in a vacuum environment is described herein. The heat-pipe radiator system is referred to as an optimized flight-weight-prototype fluid-header panel, or simply the prototype fluid header.

The study included performance evaluations over a wide range of coolant inlet temperatures, coolant flow rates, and environmental absorbed heat fluxes. The maximum performance of the system was determined.

The prototype fluid-header results were compared with a) earlier data obtained on the smaller fluid-header feasibility panel, and b) computer predictions.

The study included a description of freeze-thaw tests and an evaluation of the change in thaw recovery time due to the addition of a low-freezing point feeder heat pipe.

Experimental panel fin-temperature distributions were compared with calculated results.

TABLE OF CONTENTS

LIST OF FIGURES

List of Figures (Continued)

List of Figures (Continued)

LIST OF TABLES

1.0 INTRODUCTION

This is the fourth annual report describing analytical effort under contract NAS9-13844 in support of a NASA research investigation pertaining to heat-pipe radiators for waste heat rejection in space. Earlier reports (1, 2, 3) featured analytical and experimental comparisons of vacuum chamber data obtained on a feasibility 8 ft x 4 ft radiator panel, built and designed by Grumman Aerospace Corporation (4). Described in those reports were computer models for predicting the panel's steady-state and transient performance. NASA's testing program included freezing and thawing of the panel (2).

Heat pipes, as a means of isothermal and thermal control, are near ideal for spacecraft support equipment (5, 6) and their acceptance can reduce power requirements, cost, noise and vibration. An attractive feature is that heat pipes have high reliability, since they are self-contained and have no moving parts. Zero-gravity environments actually improve their operation (7, 8). The initial utilization of heat pipes in space, either experimentally or as functional components, have consistently given encouraging results (7, 9).

One method of heat-pipe control is referred to as the variable-conductance heat pipe (VCHP). By combining an inert gas with the working fluid the active portion of the heat-pipe condenser is established by the location of the inert gas and working fluid interface which is a function of the heat load (10).

The feasibility panel, Fig. 1.1, which utilized the VCHP concept was tested in a large thermal vacuum chamber. The system included a fluid-loop heat exchanger, a VCHP header, and conventional feeder heat pipes to drive the radiating fins. An analysis of the VCHP data is contained in references 1, 2, and 3. A major finding of the experimental program was that under most conditions the active portion of the VCHP header condenser was less than predicted, which resulted in low heat transport compared to analysis. Due to the sub-marginal VCHP performance, NASA decided to temporarily abandon the VCHP and concentrate on a fluid header with heat-rejection control provided by fluid modulation. The VCHP was converted into a fluid header (feasibility fluid header) and retested. No alteration was made to the feeders and panel.

Grumman Aerospace Corporation who had designed and built the VCHP later constructed a larger 6 3/4 ft by 10 2/3 ft heat-pipe radiator panel, Fig. 1.2, (prototype fluid header). A computer thermal model for fluid-header radiator panels was written at Tuskegee Institute and results from a parametric systems analysis obtained (3).

Described in the present report are the principal results from a two-week testing program of the prototype panel in a thermal vacuum chamber at L. B. Johnson Space Flight Center. In late 1977, a modular heat pipe radiator system consisting of three prototype panels is scheduled to be tested.

As mentioned above, the tests on the VCHP panel and the VCHP panel reworked into a fluid header included freeze-thaw cycles. The panel was consistently difficult to thaw, requiring as much as 9 to 10 hrs to re-

HEAT PIPE RADIATOR

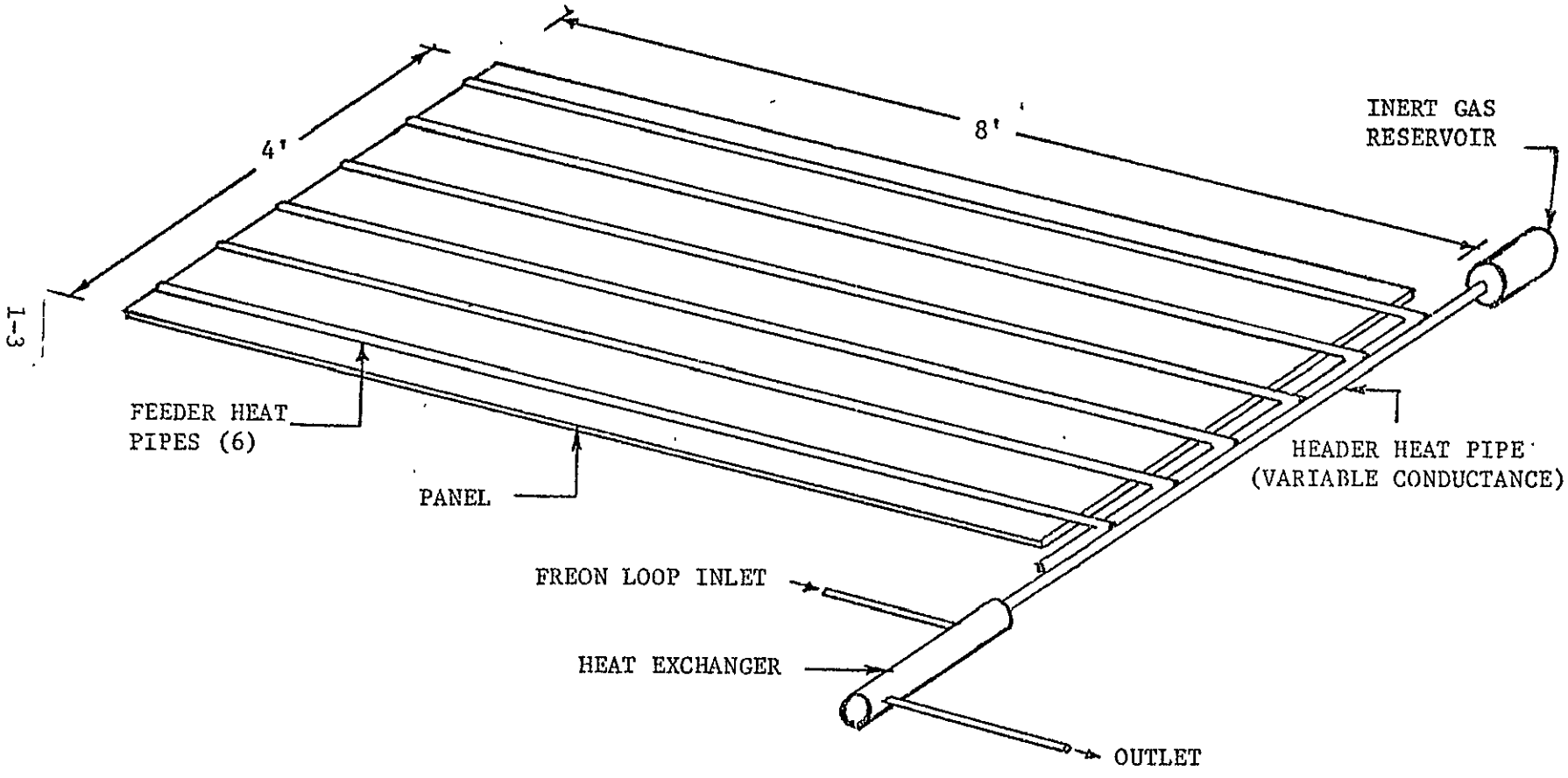

Figure 1.1. VCHP with Feeder Heat Pipes and Panel

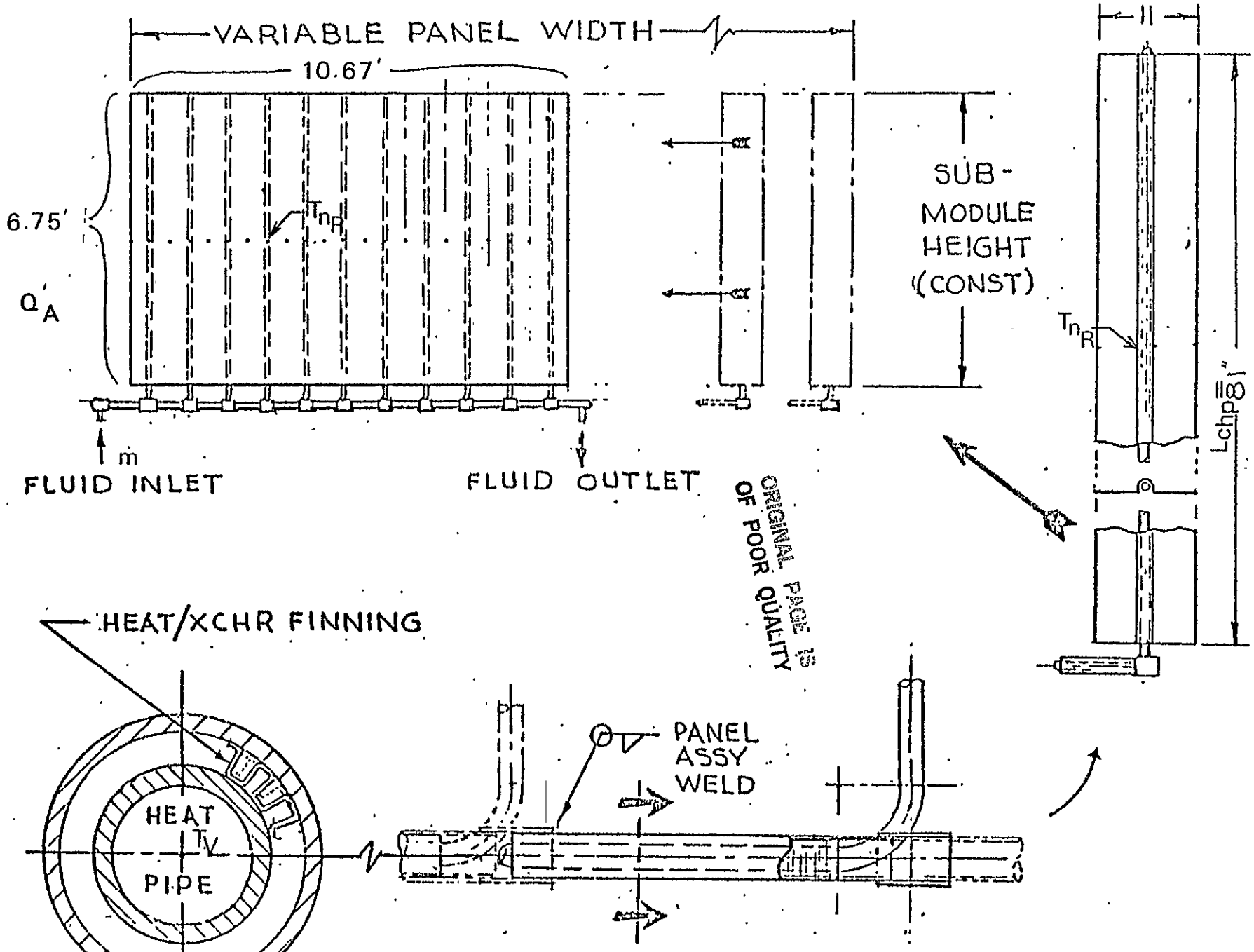

Figure 1.2. MODULAR FEEDER HEAT PIPE RADIATOR SYSTEM

cover from a hard freeze. It was thought that the addition to the prototype panel of a propane heat pipe which would not freeze but would operate continuously, even when the ammonia heat pipes were frozen, would substantially reduce the thaw time. A determination of the value of the propane heat pipe was an important objective of the tests.

2.0 PERFORMANCE

2.1 Comparison with computer predictions

A total of approximately 60 tests on the prototype panel were made. The operating conditions for 34 of the steady-state prototype test points have been run on the computer (3) and the results compared with the corresponding experimental data, Table 2.1. The experimental heat rejection values determined from $\Sigma\sigma\bar{T}_p^4$ were in better agreement with the computer program results than when calculated from $\dot{m}c_p\Delta T$. The calorimetric method is expected to be the more accurate, however, since the fluid ΔT was measured directly with a differential temperature transistor, whereas the average panel temperature $\bar{T}_p$ was estimated from only a limited number of thermocouples, Fig. 2.15. The average percent deviations from the predicted performance were 9 and 6 for the two methods, respectively, which in either case is considered satisfactory for heat-transfer experiments. In the 34 tests of Table 2.1, the experimental Q_{REJ} values were higher than calculated in 11 of the tests when determined by $\dot{m}c_p\Delta T$ and in 21 tests from $\Sigma\sigma\bar{T}_p^4$. Because of the good agreement, it is difficult to ascertain whether the discrepancy that did exist was primarily due to insufficient instrumentation or errors either in the experimental data or in the computer thermal model.

2.1.1 Effect of T_{IN} on Q_{REJ}

The effect of variation of T_{IN} on Q_{REJ} ($\dot{m} \simeq 500$ LB/HR and $Q_A \simeq 60$ BTU/HR-FT^2 is presented in Fig. 2.1 for values of T_{IN} = 50, 100 and 150°F. The experimental results are slightly under the calculated

TEST PT.	TIME	T_{IN} °F	$\dot{m}$ LB/HR	Q_A BTU/HR-FT^2	Q_{REJ}, BTU/HR			% DEV.	
					EXP		CALC		
					$\dot{m}c_p\Delta T$	$\Sigma\sigma T_p^4$		$\dot{m}c_p\Delta T$	$\Sigma\sigma T_p^4$
F I R S T W E E K									
101	125/02/27	49.7	499	23.4	3300	3590	3538	-7	-.4
104	125/05/00	51.1	1015	26.0	3700	3820	3728	-1	-.9
107	125/07/15	49.7	1986	25.6	3810	3990	3854	-1	.3
108	125/10/00	100.9	2011	26.0	6150	6160	5717	7	6
105	125/12/59	100.2	1002	24.5	5920	5840	5371	9	4
102	125/14/58	99.5	501	23.9	4662	5290	4957	-6	4
103	125/20/57	149.3	505	27.1	6575	6990	6421	2	4
106	125/22/45	150	1002	28.1	7600	7540	7001	8	2
109	126/01/12	149.3	2011	25.4	7900	7240	7677	3	-8
120	126/05/09	149.3	2011	60.1	6410	6400	6300	2	-1
117	126/06/58	149.3	989	63.6	5900	6090	5617	5	2
114	126/08/45	149.3	501	64.8	5160	5680	5053	2	6
111A	126/12/30	104.3	254	56.8	3090	3400	3268	-6	1
113	126/14/06	98.8	501	58.0	3250	3850	3567	-9	4
116	126/15/00	99.5	989	57.5	3970	4170	3943	1	1
119	126/16/15	99.5	2024	57.3	4140	4460	4268	-3	2
115	126/19/30	49.7	989	56.4	2000	2290	2239	-12	-1
112	126/21/00	50.4	503	59.9	1700	1930	1934	-14	-2
111	126/22/30	80.8	248	58.6	2390	2560	2533	-6	-1
126	127/02/55	150.0	2011	80.0	5200	5890	5502	-6	4
125	127/05/55	100.2	2011	81.1	3100	3350	3192	-3	3
124	127/07/15	50.4	1986	77.1	1180	1350	1331	-13	-2
123	127/09/30	149.3	496	112.3	3810	3990	3310	13	-15
122	127/12/40	-0.1	505	90.3	-950	-570	-1046	-10	-66
127	127/18/33	49	2011	8.5	4840	4610	4618	5	-3
128	127/19/48	100.9	2011	11.3	7050	6420	6315	10	-.1
129	127/21/05	125.1	2011	12.7	8240	7310	7168	13	0
130	127/22/05	150	2024	14.1	9620	8200	8112	17	1
131	128/00/30	150.0	2779	12.4	8330	7370	8314	-.2	-14
S E C O N D W E E K									
214	140/13/21	147.6	2011	59.9	7090	6950	6232	12	9
213	140/14/06	99.0	1999	58.7	3960	4670	4180	-6	9
212	140/15/51	50.4	2011	57.7	1540	2570	2306	-49	7
210	141/14/24	56.0	2011	8.1	5370	5660	4847	10	5
210B	141/15/39	150.2	2063	12.7	10000	8780	8176	18	5

TABLE 2.1. Comparison of Experimental and Calculated Prototype Panel Data; 34 Test Points.

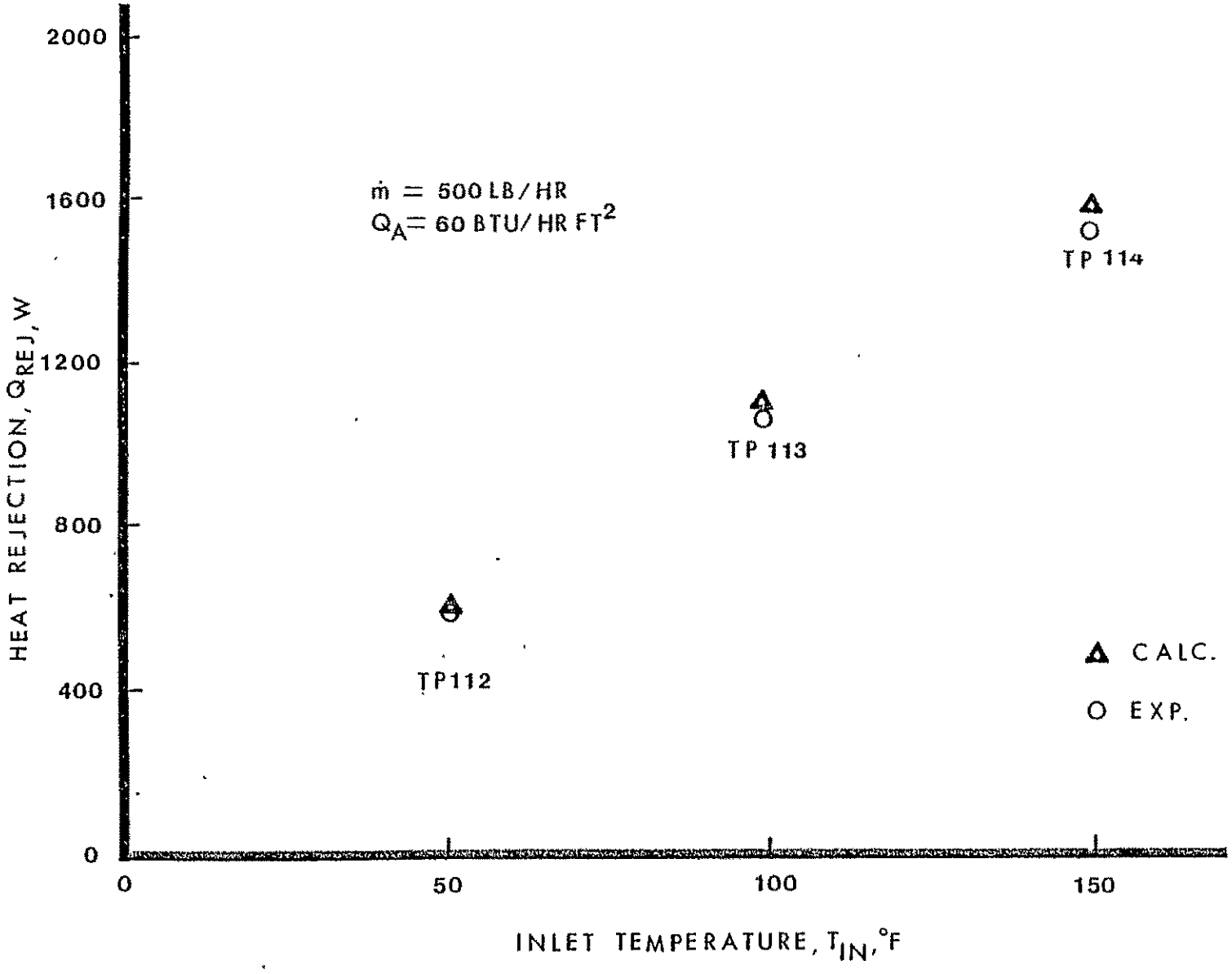

Figure 2.1 The effect of T_{IN} on Q_{REJ}: $\dot{m}$ = 500 LB/HR, Q_A = 60 BTU/HR-FT^2.

data from the computer thermal model, but both indicate that T_{IN} has a strong and approximately linear effect on Q_{REJ}.

2.1.2 Effect of $\dot{m}$ on Q_{REJ}

When T_{IN} was maintained constant at 100°F and the heat absorbed held at 60 BTU/HR-FT^2, a variation of the freon flow rate from 250 to 2000 LB/HR increased the heat rejected, but not by a large factor, Fig. 2.2, which is again in agreement with the calculations.

2.1.3 Effect of Q_A on Q_{REJ}

The expected strong dependency of Q_{REJ} on the absorbed heat flux was verified by the experiments. With T_{IN} = 150°F and $\dot{m}$ = 500 LB/HR, a decrease of Q_A from 110 to 25 BTU/HR-FT^2 increased Q_{REJ} by about 63 percent, Fig. 2.3.

2.2 Comparison with fluid header feasibility panel results

2.2.1 Performance

Near identical operating conditions existed for both the prototype and feasibility fluid header in three tests. Table 2.2 presents a comparison of the performance data for those runs. In Figs. 2.4, 2.5, and 2.6 the vapor, and panel temperature distribution for the six tests are presented. It is of interest to note that on the basis of the heat rejection parameter Q_{REJ}/A, Table 2.2, the earlier feasibility fluid header panel,(Fig. 1.1), values were similar to the later prototype panel which featured finned evaporators emmersed into the coolant for enhanced heat transfer, Fig. 1.2. The explanation for the similar heat

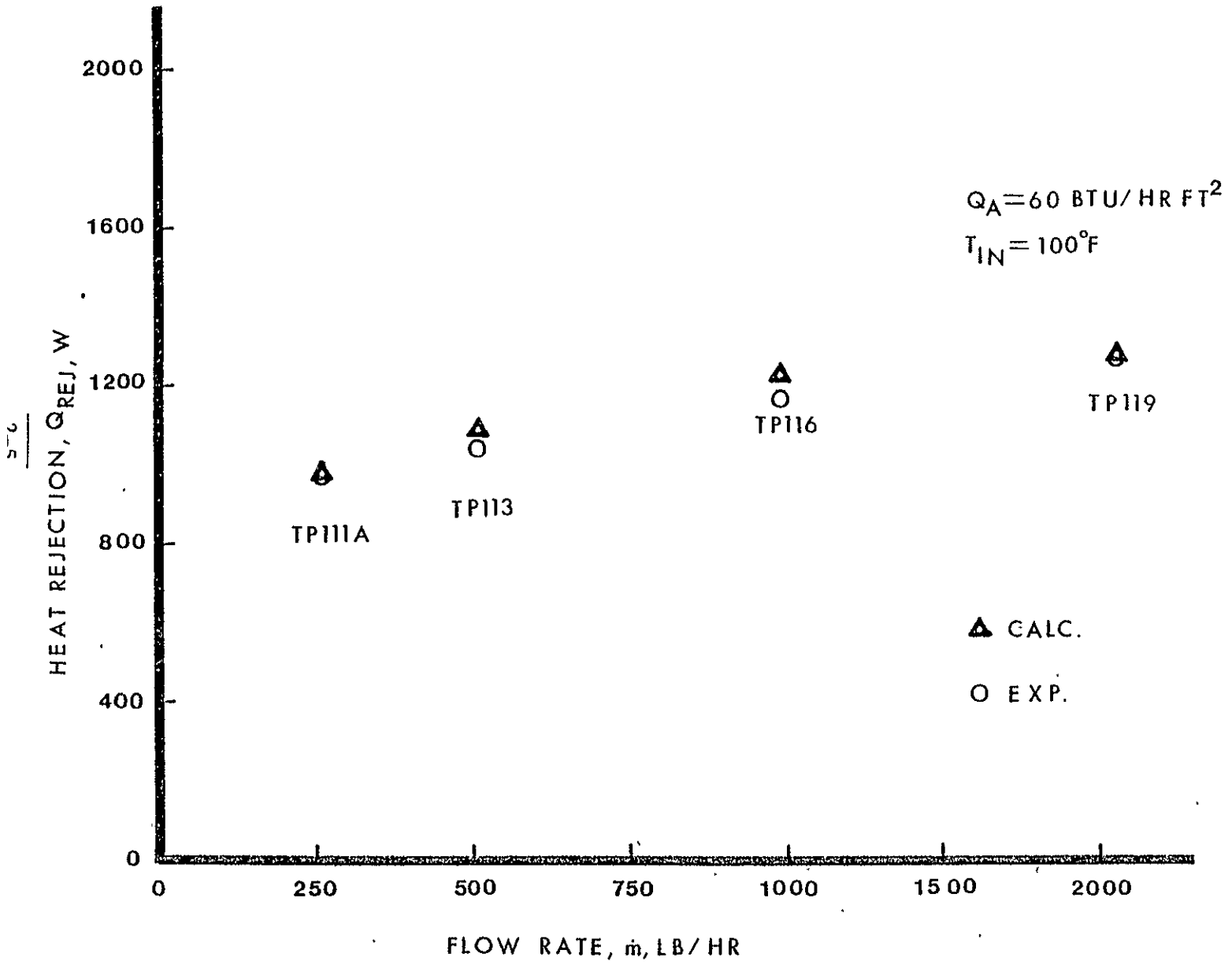

Figure 2.2 The effect of ṁ on Q_{REJ}: T_{IN} = 100°F, Q_A = 60 BTU/HR-FT^2

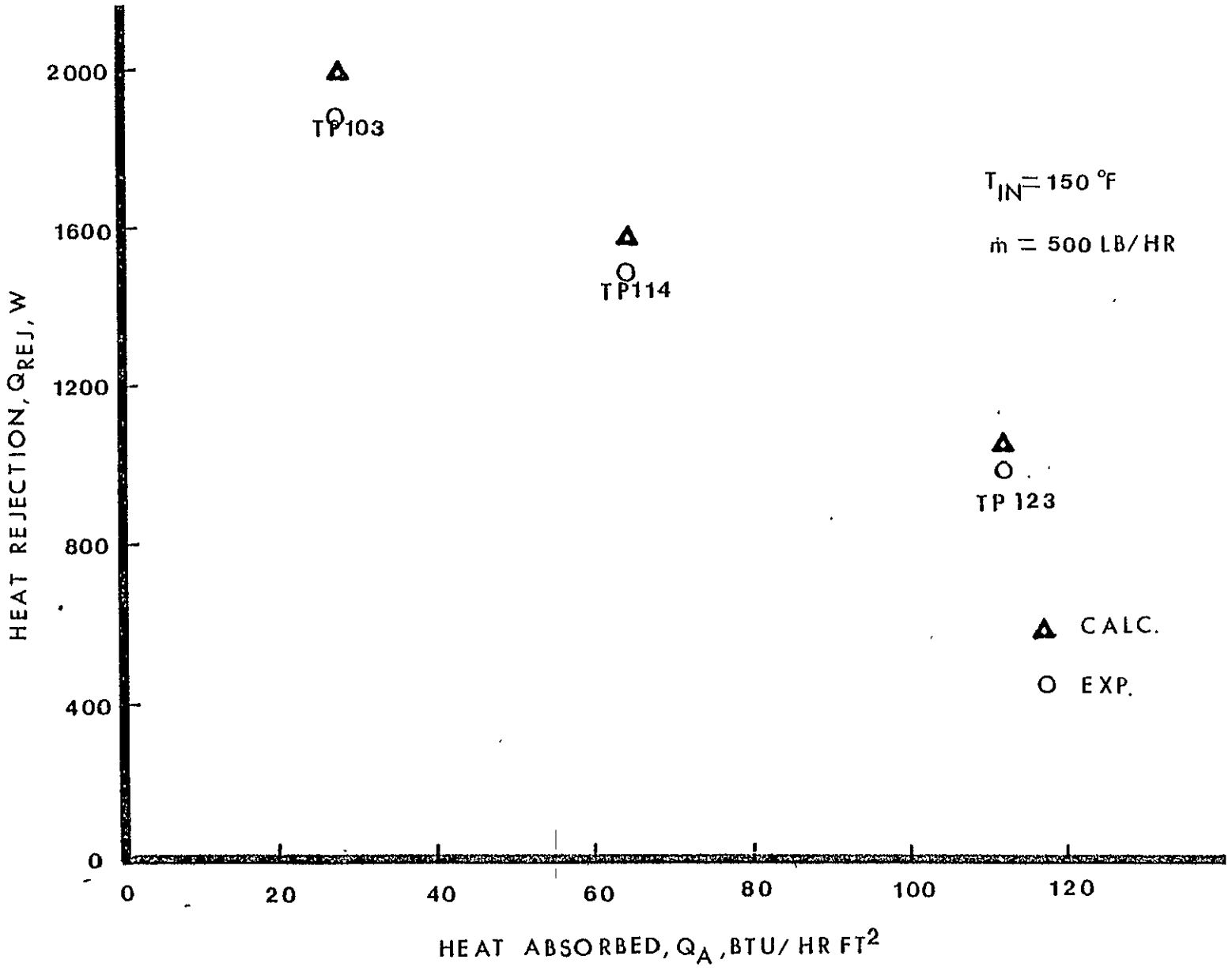

Figure 2.3 The effect of Q_A on Q_{REJ}: $\dot{m}$ = 500 LB/HR.

TEST PT.	TIME	PANEL TYPE	T_{IN} °F	$\dot{m}$ LB/HR	Q_A $\frac{BTU}{HR-FT^2}$	Q_{REJ} BTU/HR		Q_{REJ}/A WATTS/FT^2		Q_{REJ}/W WATTS/LB	
						EXP ($\dot{m}C_p\Delta T$	CALC.	EXP.	CALC.	EXP.	CALC.
12A	231-02-25	Fluid-Header Feasibility Panel	150.9	519	63.7	2323	2555	21	23	19	21
114	126-10-00	Prototype	149.3	501	64.8	5160	5053	20	20	24	23
17	233-00-27	Fluid Header Feasibility Panel	150.9	1990	22.9	4179[?]	3523	38[?]	31	34[?]	29
109	126-01-15	Prototype	149.3	2011	25.4	7900	7677	31	29	36	35
6A	231-00-56	Fluid-Header Feasibility Panel	98	1016	59.4	1594	1751	15	16	13	14
116	126-15-00	Prototype	99.5	989	57.5	3970	3943	16	15	18	18

TABLE 2.2. Comparison of Prototype Panel Performance with Earlier Fluid Header Feasibility Panel Results.

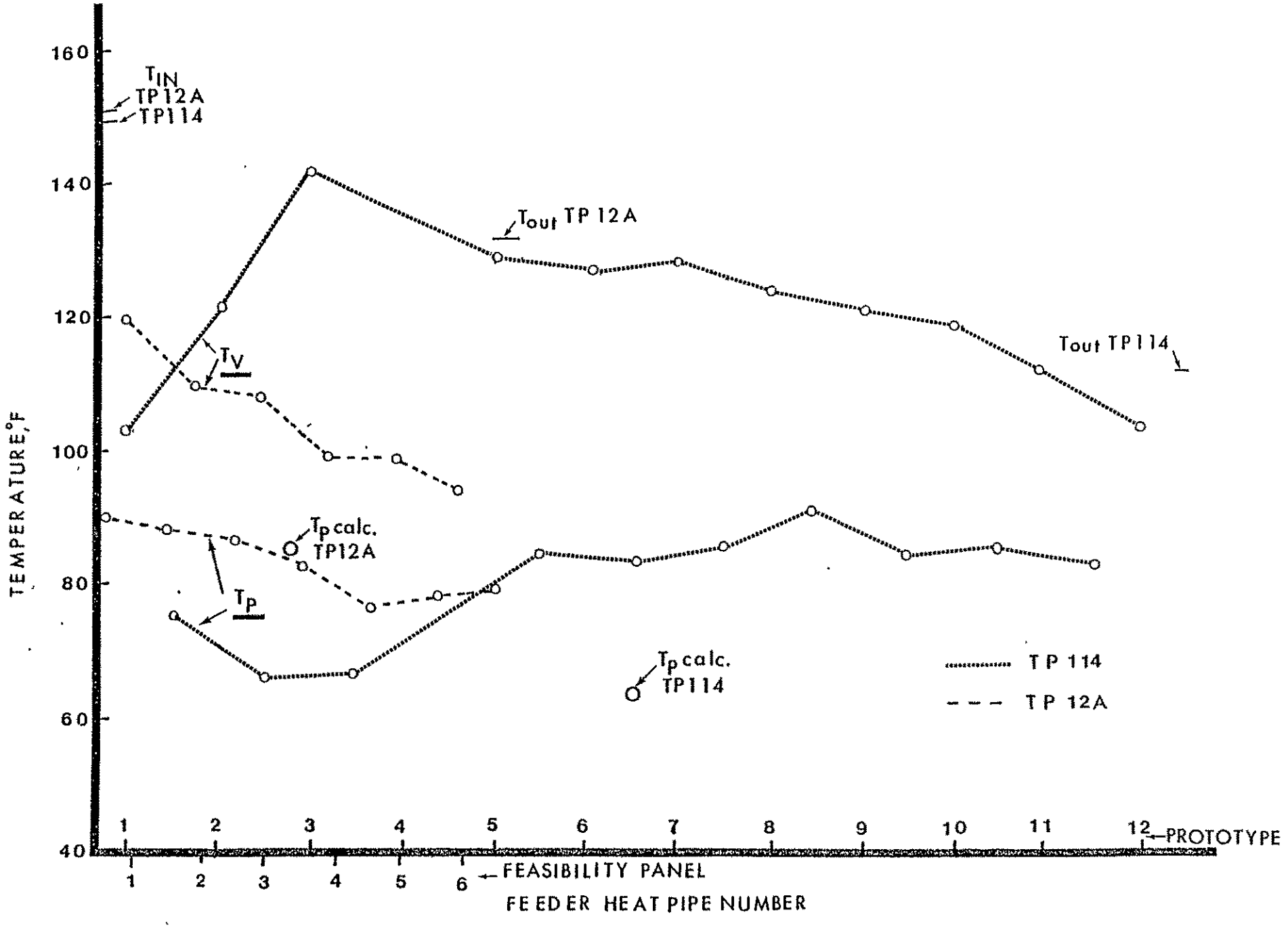

Figure 2.4 Temperature comparisons of TPs 114 and 12A.

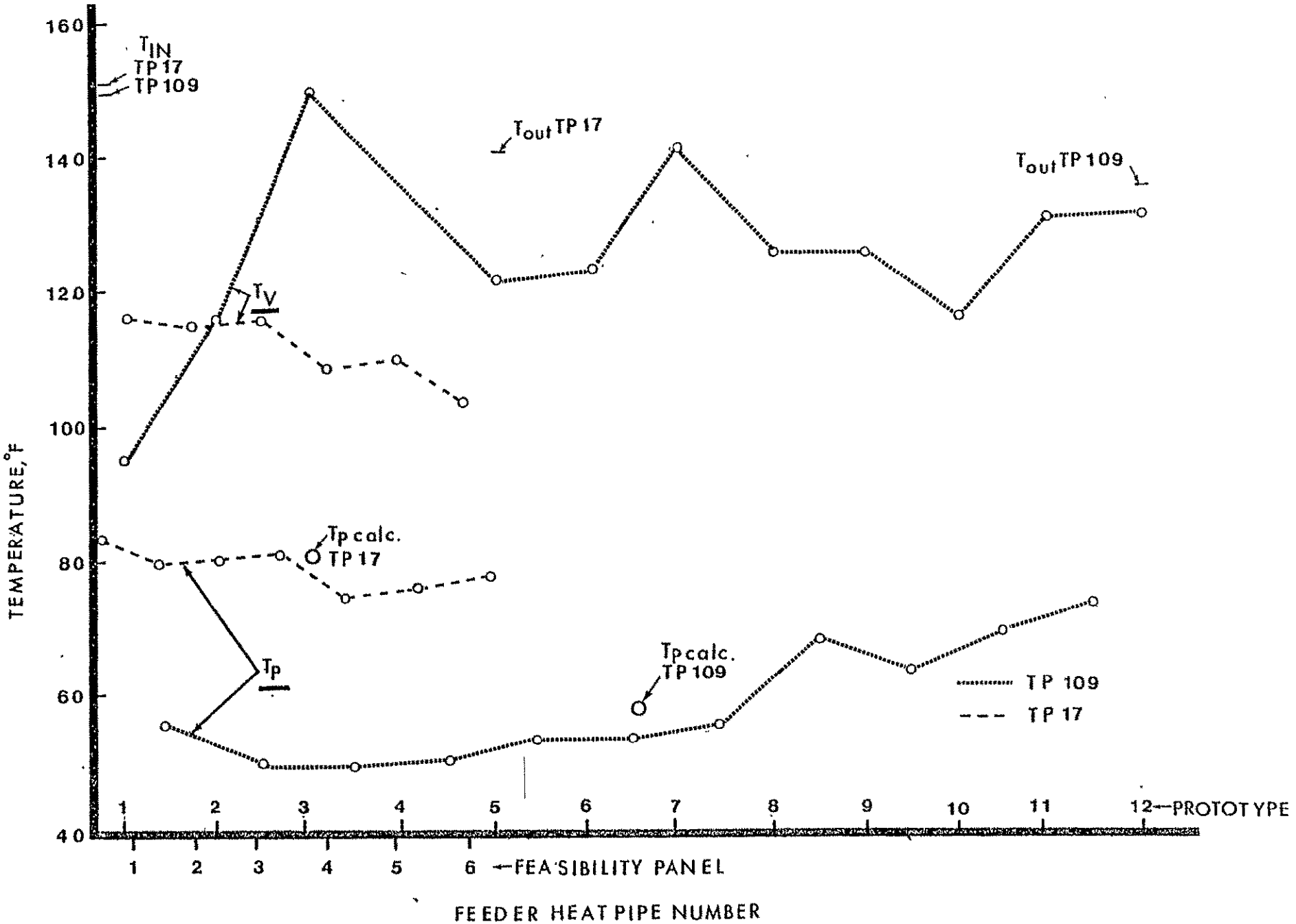

Figure 2.5 Temperature comparisons of TPs 109 and 17.

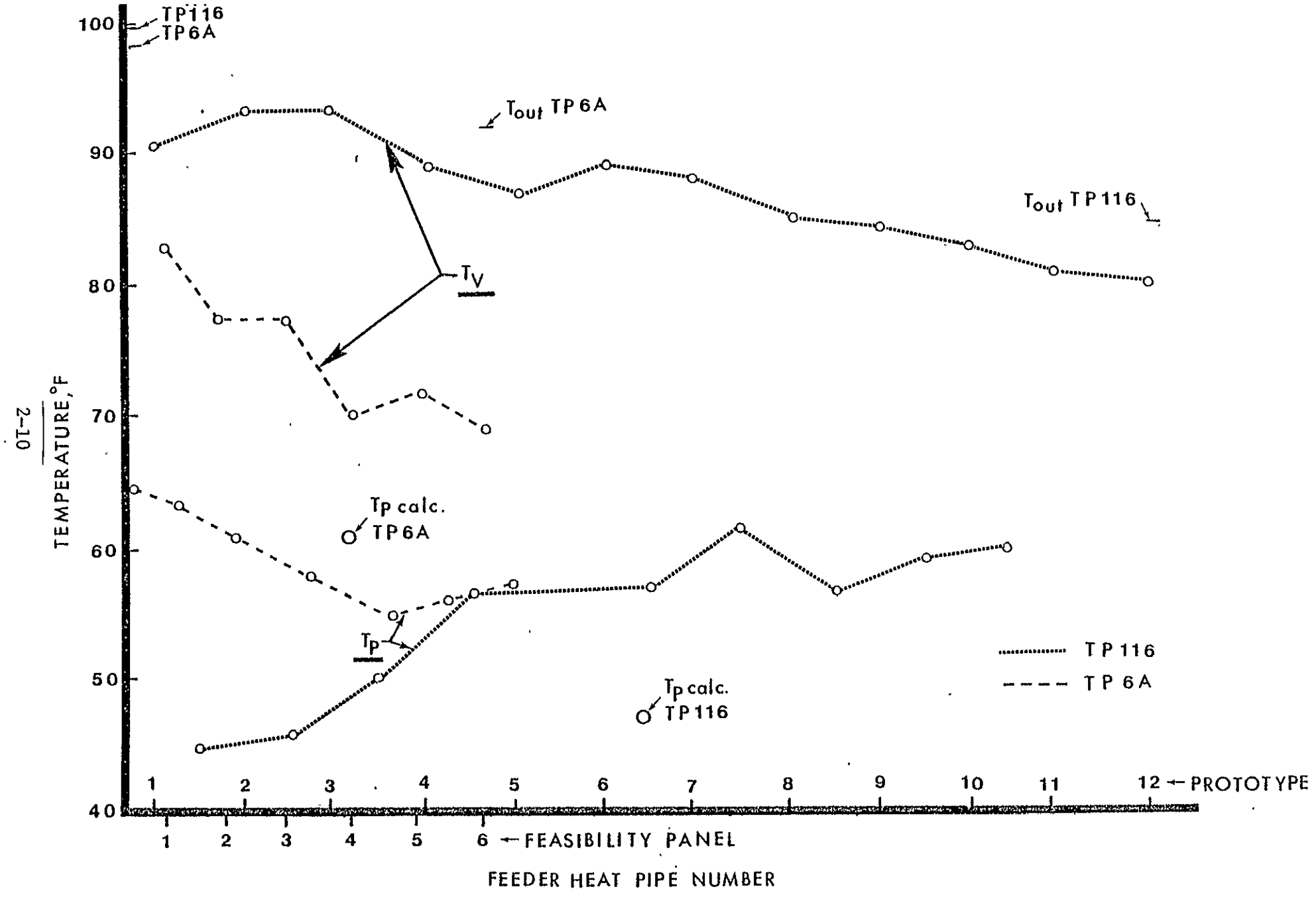

Figure 2.6 Temperature comparisons of TPs 116 and 6A.

rejection per unit area value, which was expected, is that the feeder heat-pipe spacing on the panels was less (8 compared to 11 in) for the feasibility fluid header. The closer heat-pipe spacing, however, results in a heavier radiator panel for the same heat rejection (3). A comparison of the experimental data on the basis of Q_{REJ}/W, Table 2.2, which is the more significant parameter, favors the prototype, again as expected.

2.2.2 System ΔTs

The beneficial result of placing the evaporator sections of the feeder heat pipes inside the header is manifest in the higher experimental vapor temperatures and lower $\overline{(T_{FR} - T_V)}$ drops which occured in the prototype compared to the feasibility panel fluid header for approximately the same source and sink temperatures, Table 2.3. Comparing the three experimental temperature differences of most interest, $\overline{(T_{FR} - T_V)}$, $\overline{(T_V - T_R)}$ and $\overline{(T_R - T_P)}$ with the calculated values, Table 2.3, it is apparent that much better agreement is obtained from the prototype data than was obtained on the fluid-header feasibility panel, particularly for the difference between root and panel temperatures $\overline{(T_R - T_P)}$. The better agreement is believed due to improved instrumentation for the prototype panel, especially in the measurement of T_R.

2.3 Residual effect of freeze-thaw conditions on panel performance

Subjecting the panel to several freeze-thaw cycles, to be discussed below, apparently had no detrimental residual effect on its performance. The validity of this assertion can be shown by comparing

ΔT COMPARISONS

FEASIBILITY PANEL FLUID HEADER

RUN NO.	Q_{REJ} BTU/HR	$\overline{T_{FR} - T_V}$ °F	$\overline{T_V - T_R}$ °F	$\overline{T_R - T_P}$ °F
12A	2323(2555)	35(16)	10(10)	11(24)
17	[?]4179(3523)	33(17)	18(15)	18(56)
6A	1594(1751)	19(10)	7(8)	10(16)

PROTOTYPE PANEL

RUN NO.	Q_{REJ} BTU/HR	$\overline{T_{FR} - T_V}$ °F	$\overline{T_V - T_R}$ °F	$\overline{T_R - T_P}$ °F
114	5160(5053)	(8)	13(15)	35(37)
109	7900(7677)	18(7)	25(22)	50(56)
116	3970(3943)	5(4)	10(11)	23(29)

CALCULATED VALUES IN PARENTHESIS

T_{FR} = COOLANT TEMPERATURE
T_V = VAPOR TEMPERATURE
T_R = ROOT TEMPERATURE
T_P = PANEL TEMPERATURE (MEASURED ON ℄ BETWEEN FEEDERS)

TABLE 2.3. ΔT Comparisons of Prototype Panel with Earlier Fluid-Header Feasibility Panel.

the Q_{REJ} values for the particular runs listed in Table 2.1 with similar operating conditions before and after the freeze-thaw cycles. In particular, compare:

Prefreeze-Thaw		After 2 Freeze-Thaw Cycles		After 3 Freeze-Thaw Cyles
TP 120	with	TP 214		
TP 127			with	TP 210
TP 130			with	TP 210B

In Figures 2.7, 2.8, and 2.9 a comparison of the panel temperature distributions before and after a freeze-thaw cycle is presented and it can be seen that the differences are small.

2.4 Maximum heat-transport tests

During the test program an attempt was made to determine the effective maximum heat capacity of the panel. With a low environment ($Q_A \simeq 13.5$ BTU/HR-FT^2), and a high flow ($\dot{m} \simeq 2{,}000$ LB/HR), the inlet temperature was increased in steps from 50° F to 150° F, Fig. 2.10, in a series of tests (TPs 127-130). The maximum performance (TP 130) exceeded 9,500 BTU/HR ($\simeq$ 2800W) and was obtained at the highest inlet temperature. In that test it is interesting to note that the vapor temperature distribution curve, Fig. 2.11, for the feeder heat pipes indicates that feeders #10, #6, and #11 had lower maximum output than the others. Although, as a safety precaution, inlet temperatures higher than 150° F were not investigated, it was apparent that the feeders were beginning to dry out. In fact, 10 minutes after TP 130, T_{IN} was decreased from 150° F to 127° F in 3 minutes, but then immediately brought back to 150° F at a rate of about 4.4° F/min. The panel

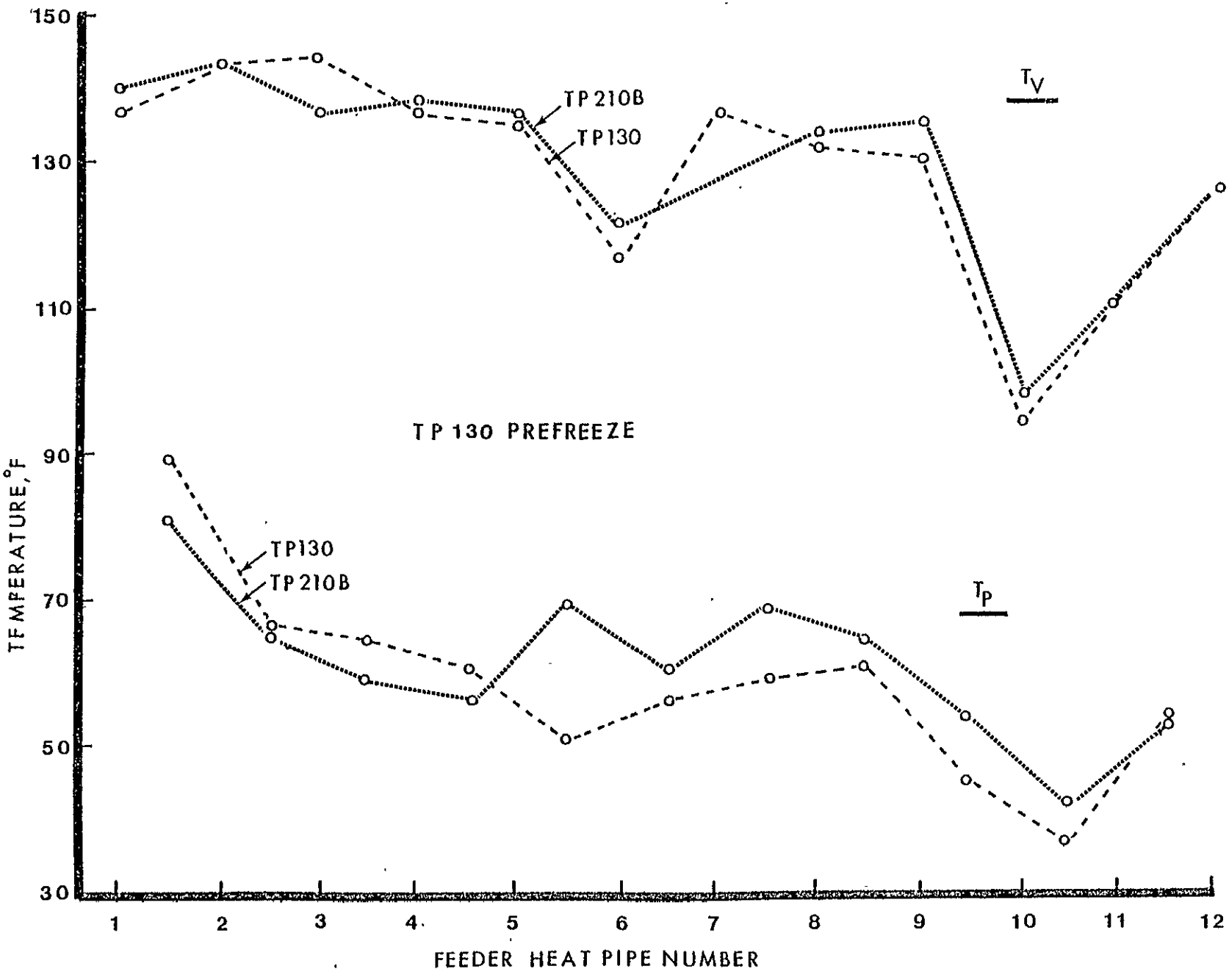

Figure 2.7 Temperature comparisons of TPs 210Band 130.

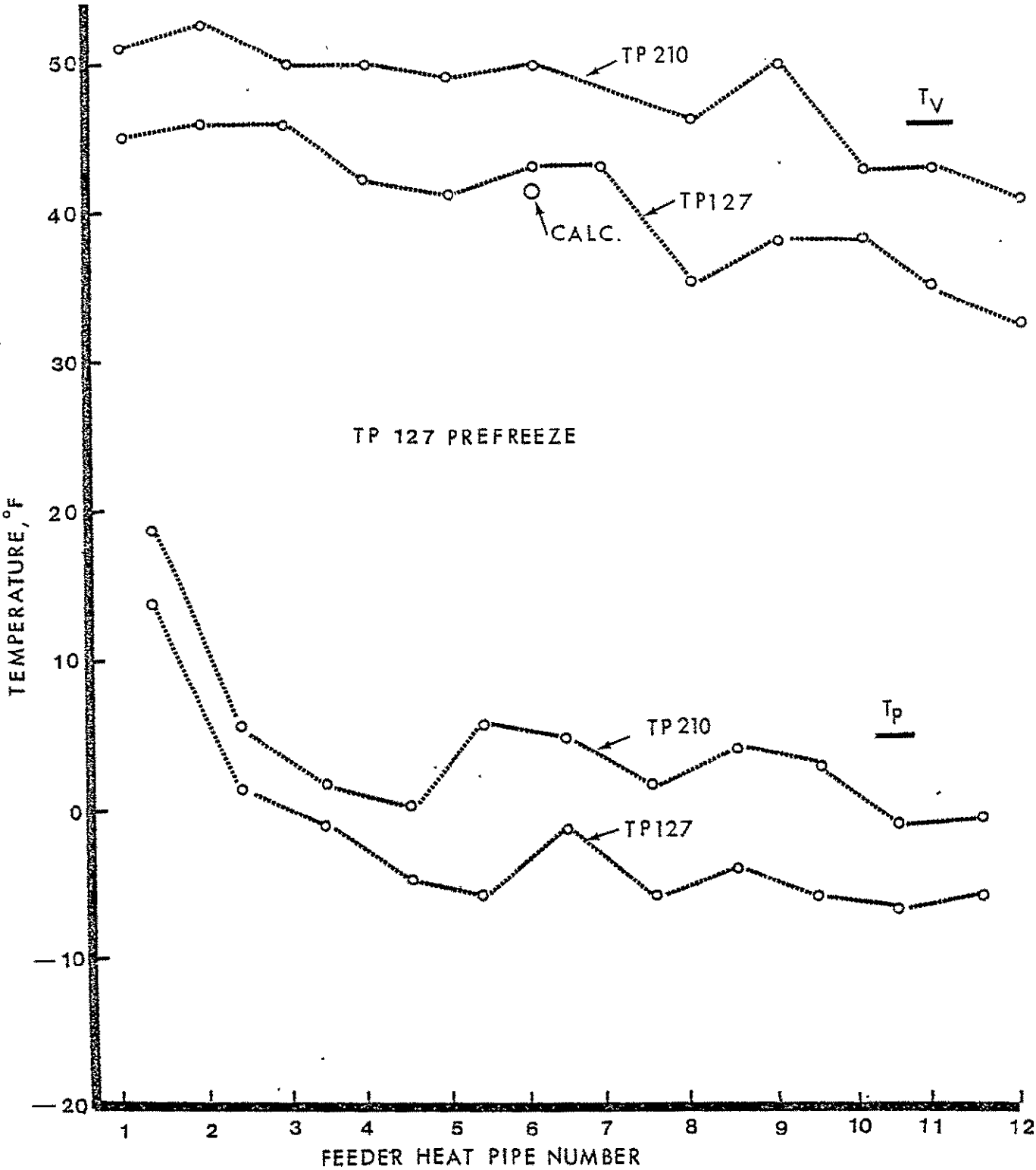

Figure 2.8 Temperature comparisons of TPs 210 and 127.

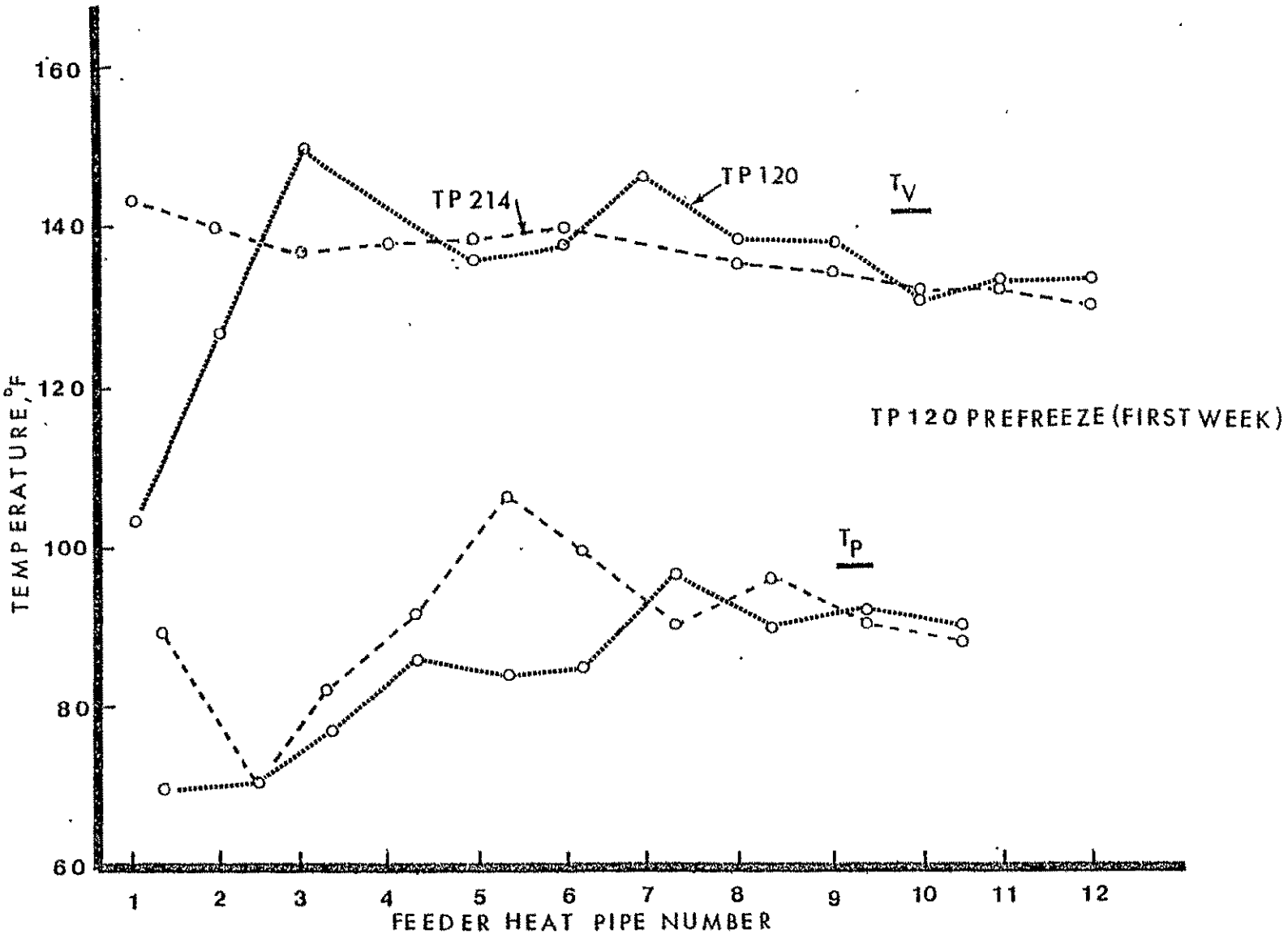

Figure 2.9 Temperature comparisons of TPs 214 and 120.

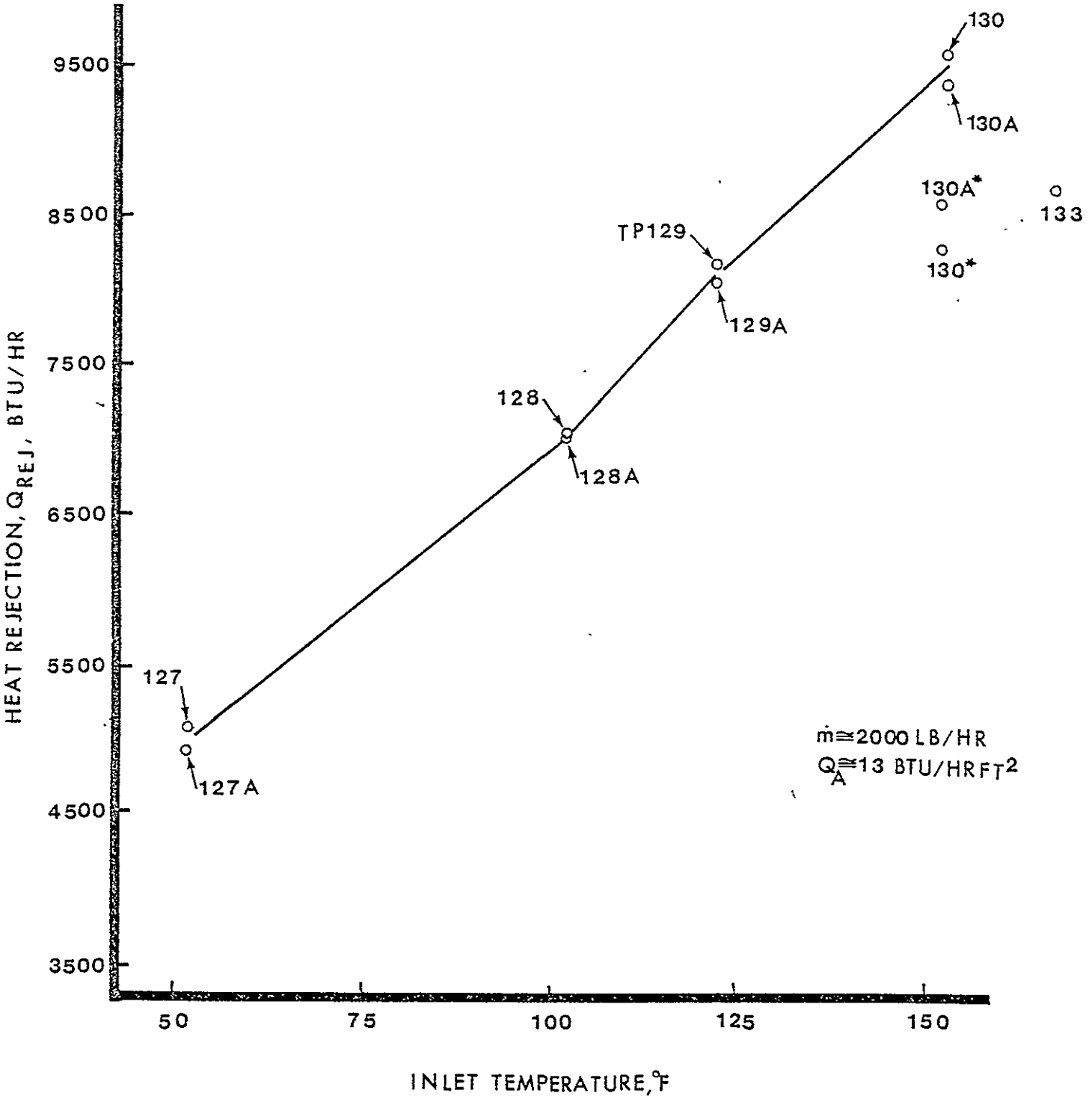

Figure 2.10 Heat pipe performance at maximum capacity.

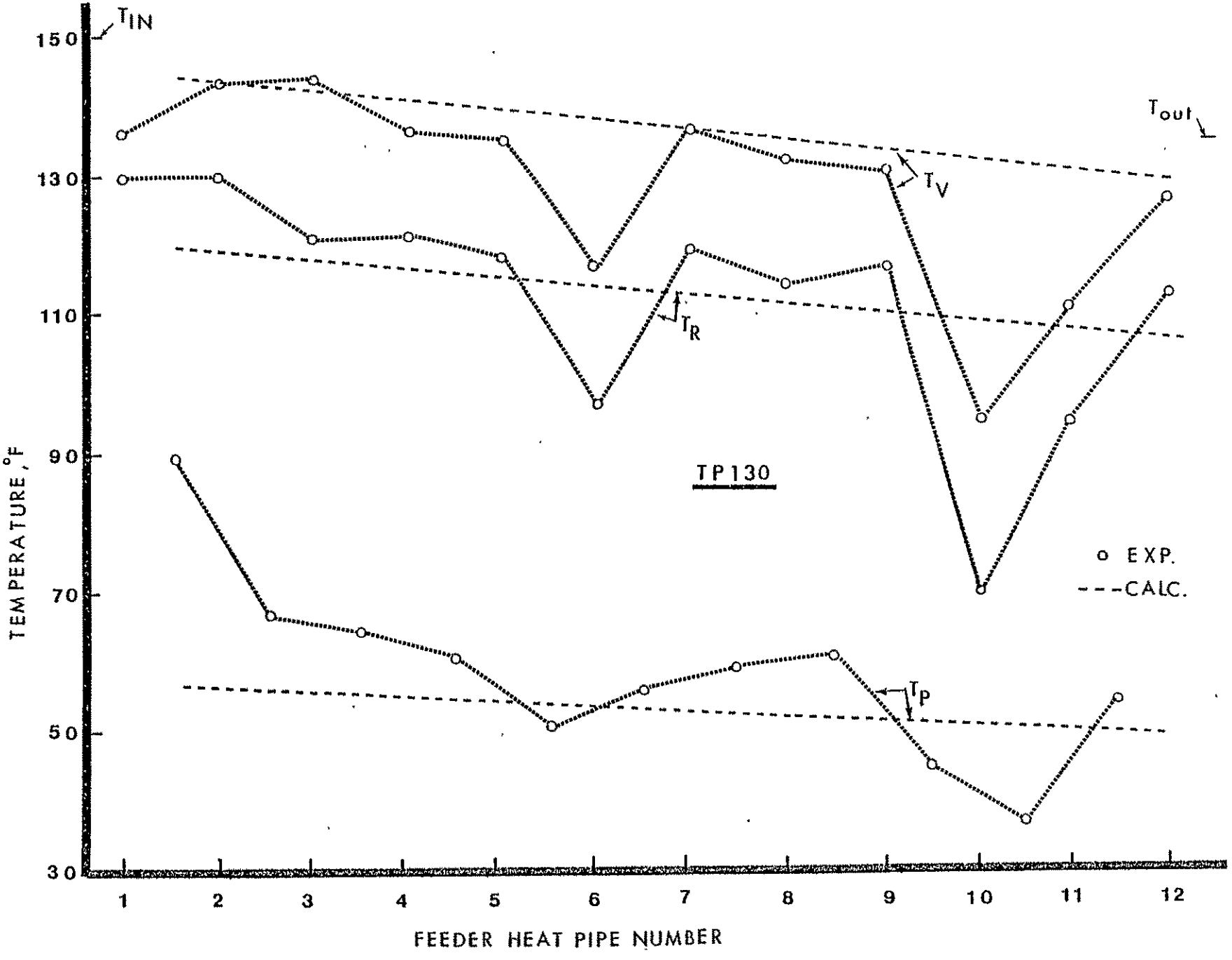

Figure 2.11 Temperature results at maximum capacity; TP 130.

performance leveled off at a value about 14% less than the Q_{REJ} for TP 130. This was TP 130*, Fig. 2.10. The only explanation that appeared logical for the inability of the panel to recover to the performance level of TP 130 was a thermal shock effect resulting from the rapid (4.4° F/min) increase of T_{IN}. The transient condition perhaps caused the wick to partially deprime with the tunnel portion of the artery the most suspect. The drops in vapor temperature between TP 130 and 130* for feeders #4 and #5 are illustrated in Fig. 2.12.

A second ramp of the inlet temperature from 50 to 150° F was conducted (TPs 127A - 130A), Fig. 2.10, and a second maximum capacity point (TP 130A) similar to TP 130 was achieved. As in the earlier ramp, however, the performance dropped to a 7% lower level (TP 130A*) after T_{IN} was decreased from 150° F to 140° F and then immediately raised back to 149° F at a rate of 2.5° F/min. Again, the loss of performance was attributed to partial depriming of the tunnel portion of the wick. It is interesting to note that the percent loss of performance was less than before, 7% compared to 14%, which may correspond to the imposing of a less severe thermal shock on the system in the second attempt 2.5° F/min compared to 4.4° F/min. The Q_{REJ} and T_V data for the maximum capacity points are summarized in Table 2.4.

2.5 Non-uniform simulator effects

Testing during week #1 revealed a temperature distribution across the IR simulator that was not as uniform as desired. Consequently, the measured panel-temperature distribution was frequently different than predicted from the computer model, Fig. 2.13, (TP 119). Occasionally,

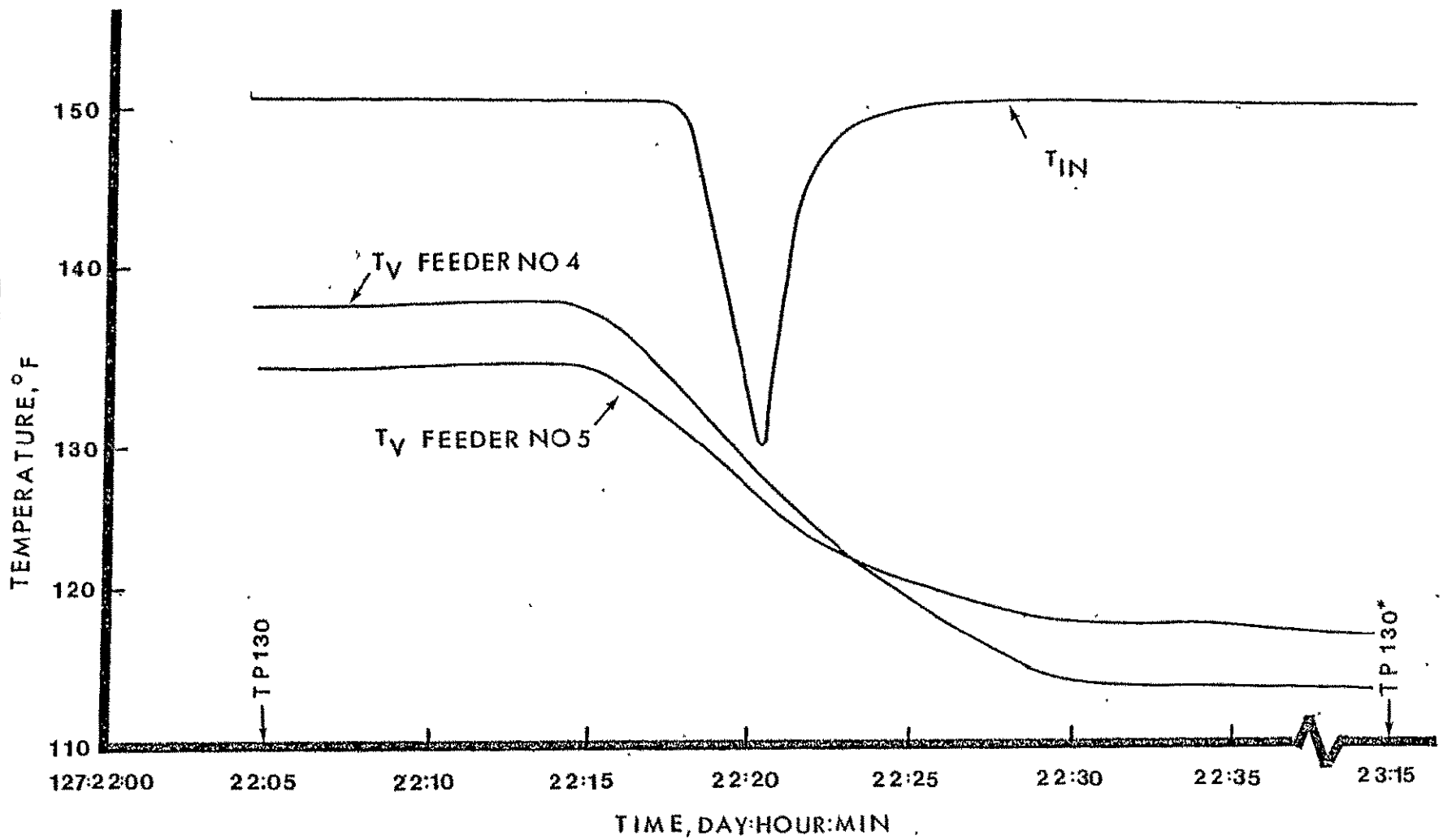

Figure 2.12. Effect of rapid change of freon inlet temperature on the vapor temperatures of feeders No. 4 and No. 5

FEEDER VAPOR TEMPERATURES, $\bar{T}_V$, °F

TP Feeder No.	130	130*	130A	130A*	133
1	137	94	137	137	135
2	142	121	142	117	123
3	144	143	144	140	-
4	137	113	138	115	-
5	135	117	135	109	113
6	114	112	116	115	122
7	137	134	137	138	145
8	131	116	118	118	123
9	130	113	130	131	146
10	93	93	96	97	103
11	111	111	110	110	115
12	127	113	127	112	111
$\bar{T}_V$ =	128	115	128	120	124

TP	TIME	T_{IN} °F	$\dot{m}$ $\frac{LB}{HR}$	Q_A $\frac{BTU}{HR-FT^2}$	$\frac{Q_{REJ}}{\dot{m}c_p\Delta T}$	BTU/HR $\Sigma\sigma \bar{T}_p^4$
130	127-22-05	150	2024	14.1	9620	9100
130*	127-23-15	150	2011	12.4	8300	8000
130A	128-08-00	150	2006	14.1	9400	9000
130A*	128-09-45	149	2005	13.2	8750	8500
133	128-11-00	165	2006	13.1	8250	8400

TABLE 2.4. Vapor temperatures and Q_{REJ} at maximum capacity conditions.

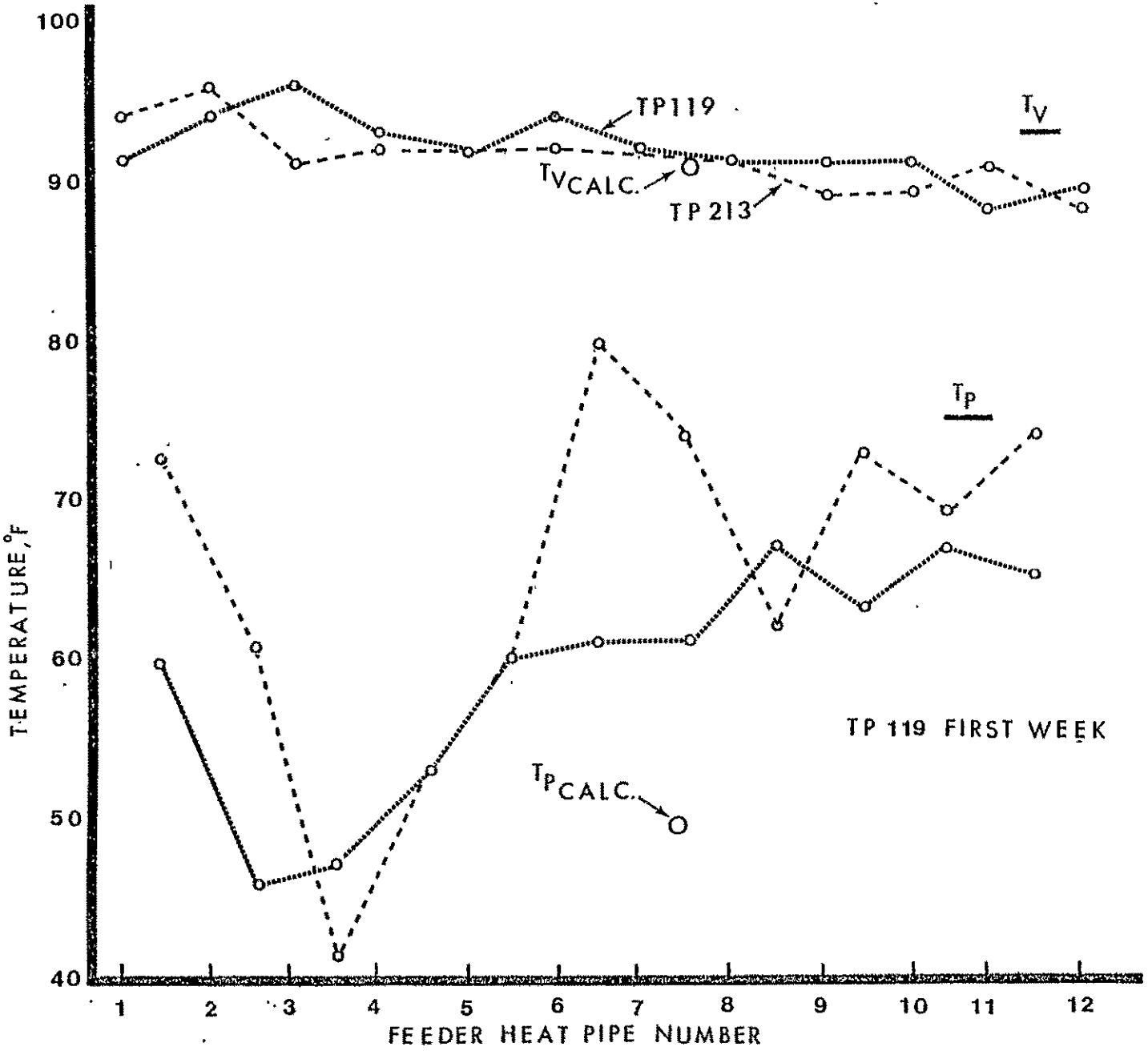

Figure 2.13. Comparison of first week and second week panel temperatures; TP 119.

however, the panel temperature distribution was nearly that calculated. Fig. 2.8, (TP 127), i.e. decreasing in the direction of freon header flow. An example of one of the more extreme mal-distributions was TP 123, Fig. 2.14. All of the 100 series tests were made during the first week of testing. For week #2, modifications to the simulator were made. The modifications did little, however, to eliminate the nonuniformities; for example, compare TP 213 with TP 119, Fig. 2.13; TP 214 with TP 120, Fig. 2.9; and TP 212 with TP 118, Fig. 2.15.

2.6 Fin-temperature distribution

An attempt was made to compare the experimental radiator fin-temperature distribution with the calculated curve. In past tests, unsatisfactory agreement had been noted (2). Therefore, before the prototype fluid-header test series, additional thermocouples were installed along the center of the panel and on two of the twenty-two panel fins: the right fin of feeder No. 2 and the left fin of feeder No. 7, Fig. 2.16.

In one combination of tests (TPs 112, 113 and 114), the heat-transfer was increased by elevating the inlet temperature, Fig. 2.1; all other conditions held constant. It was found that for the right fin of feeder no. 2 the experimental temperature measurements agreed quite well with the calculated temperature profiles, Figs. 2.17, 2.18, and 2.19. Poor agreement, however, was consistently found for the left fin of feeder No. 7, Figs. 2.20, 2.21, and 2.22, probably due to a hot region in the simulator. The problem of a nonuniform simulator was previously discussed.

It was of interest also to compare the heat transfer at the base of the fin (O.D. of the feeder) calculated from the slope of the tem-

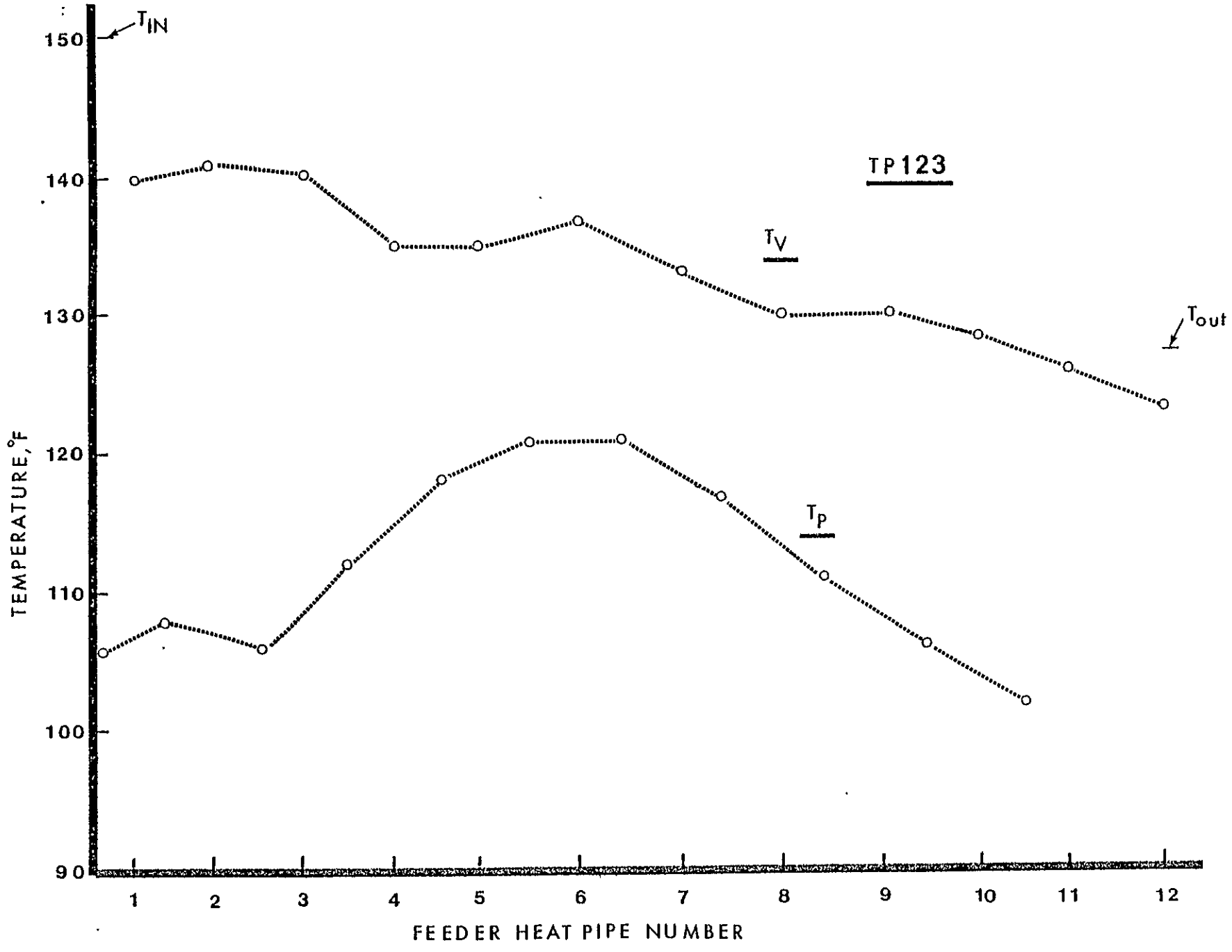

Figure 2.14. Panel temperature distribution for TP 123.

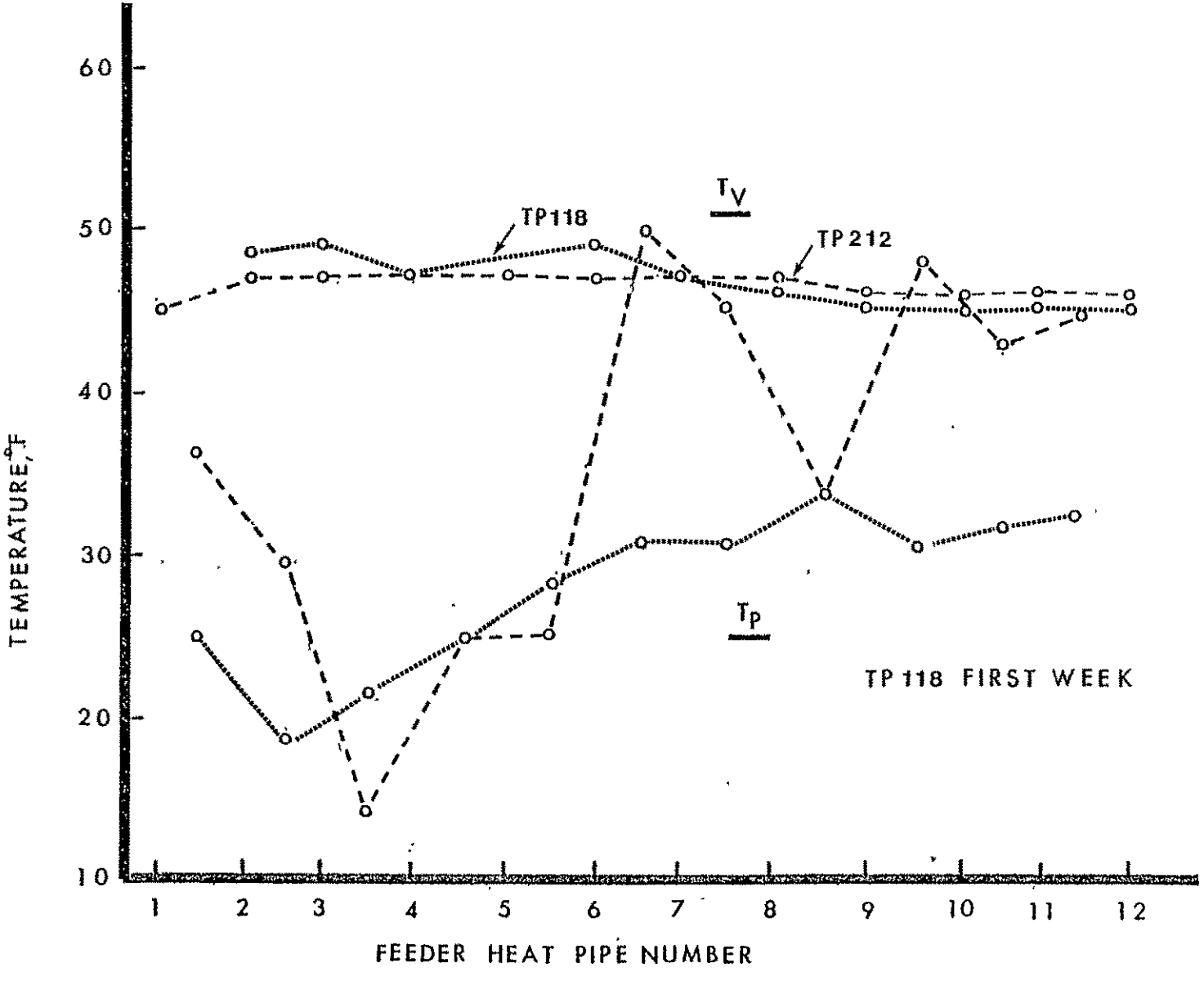

Figure 2.15. Comparison of first week and second week panel temperatures; TP 118 and TP 212.

Figure 2.16. THERMAL MAP INSTRUMENTATION

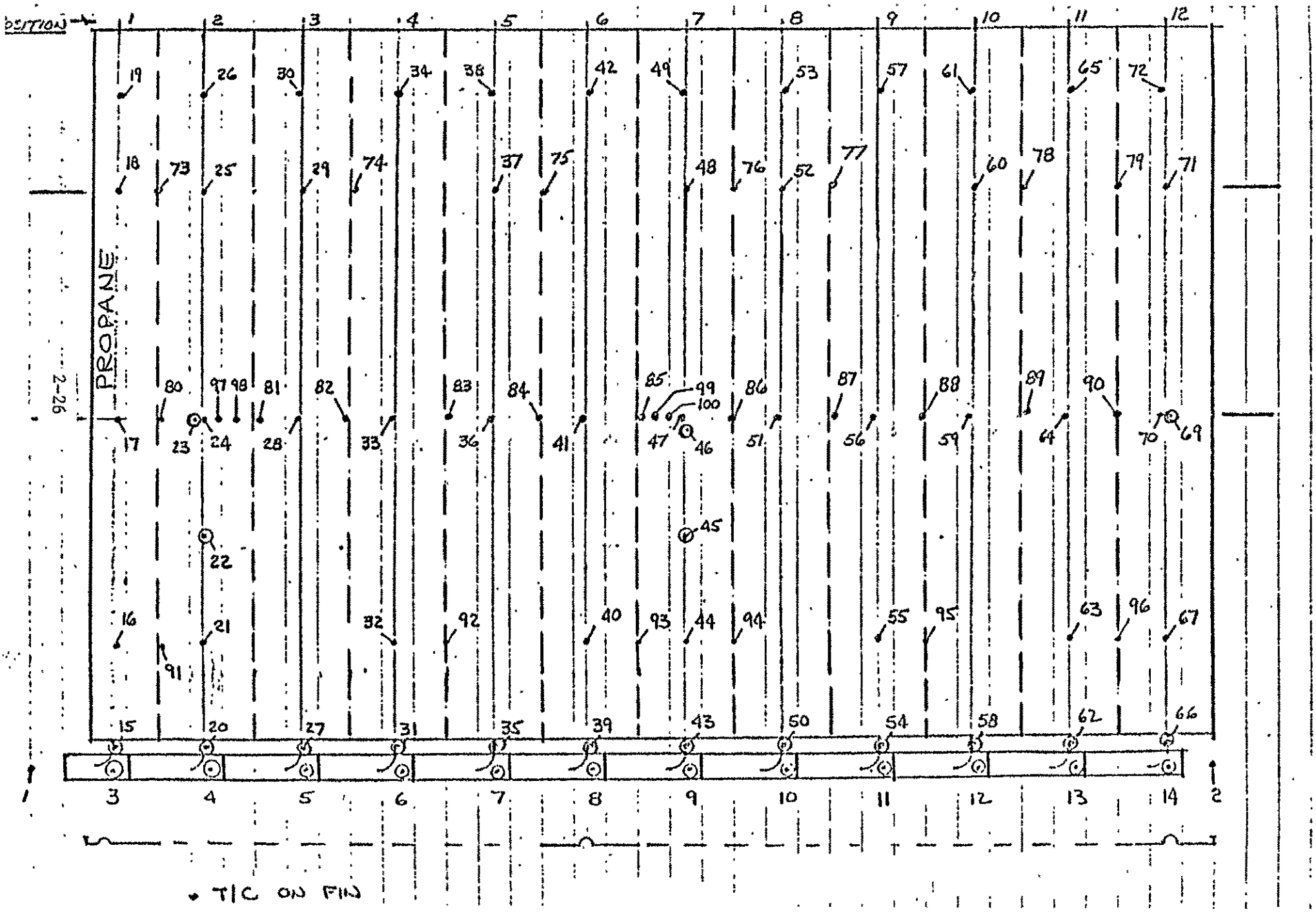

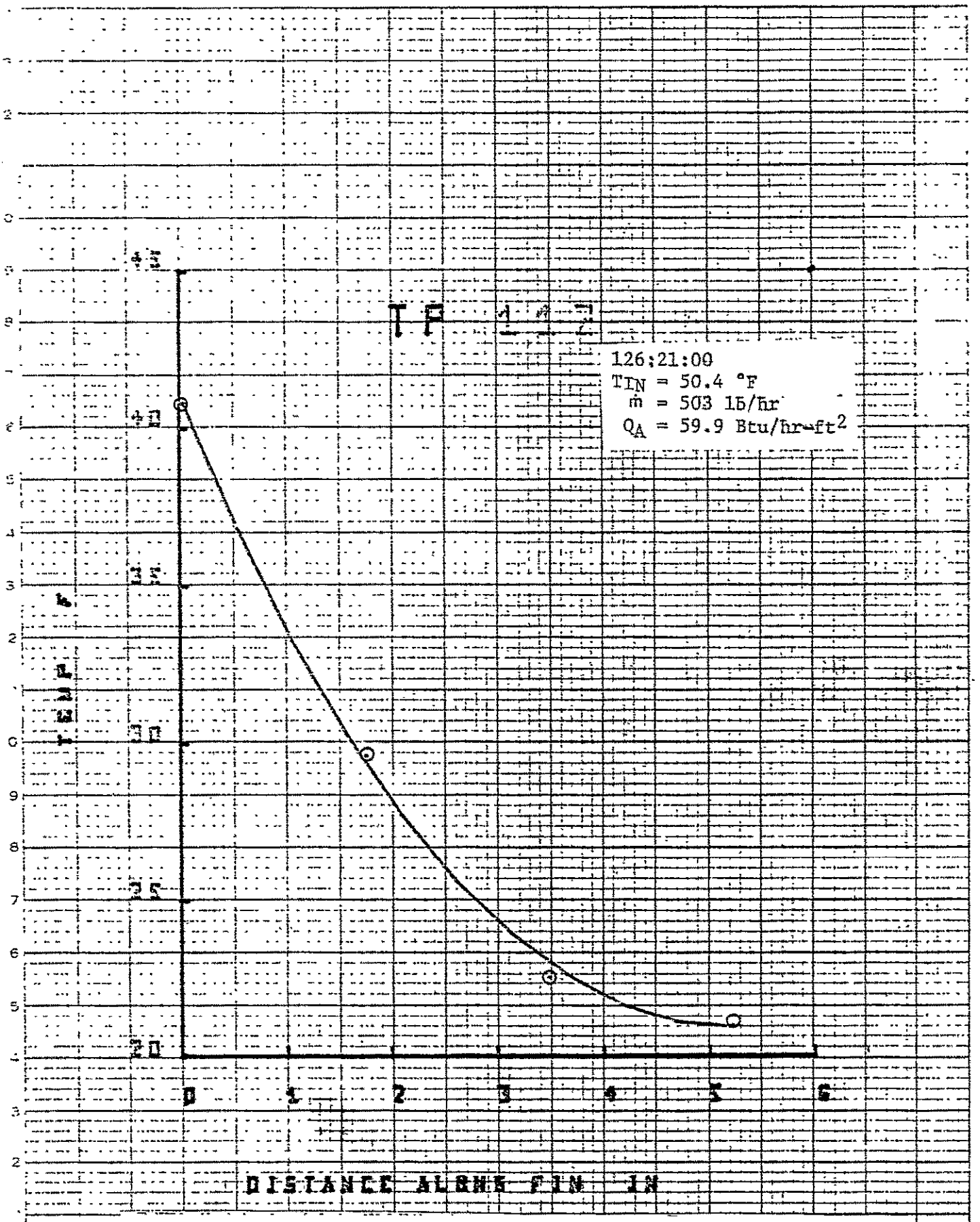

Figure 2.17 Fin temperature for right fin of feeder No. 2; TP 112.

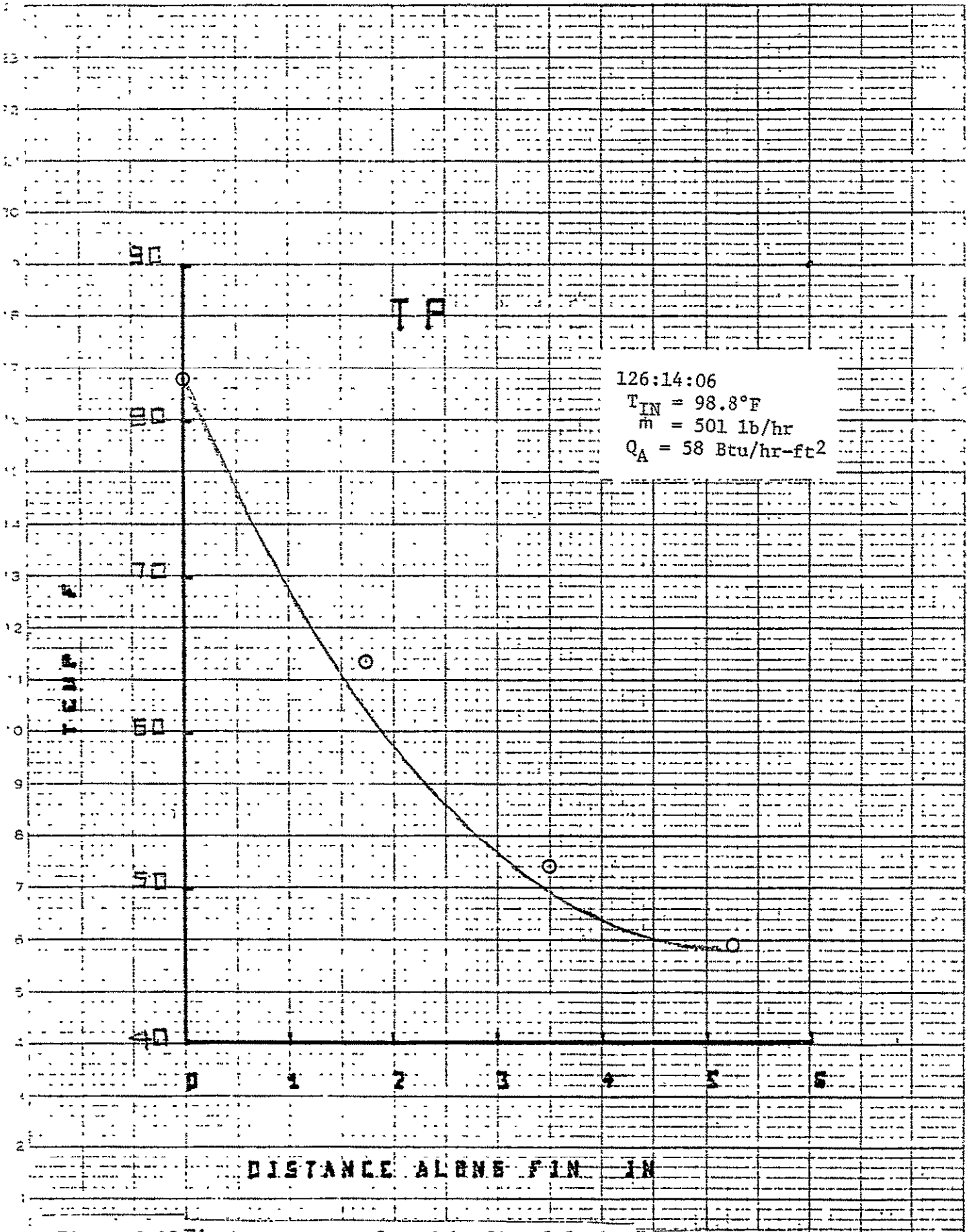

Figure 2.18 Fin temperatures for right fin of feeder No. 2; TP 113.

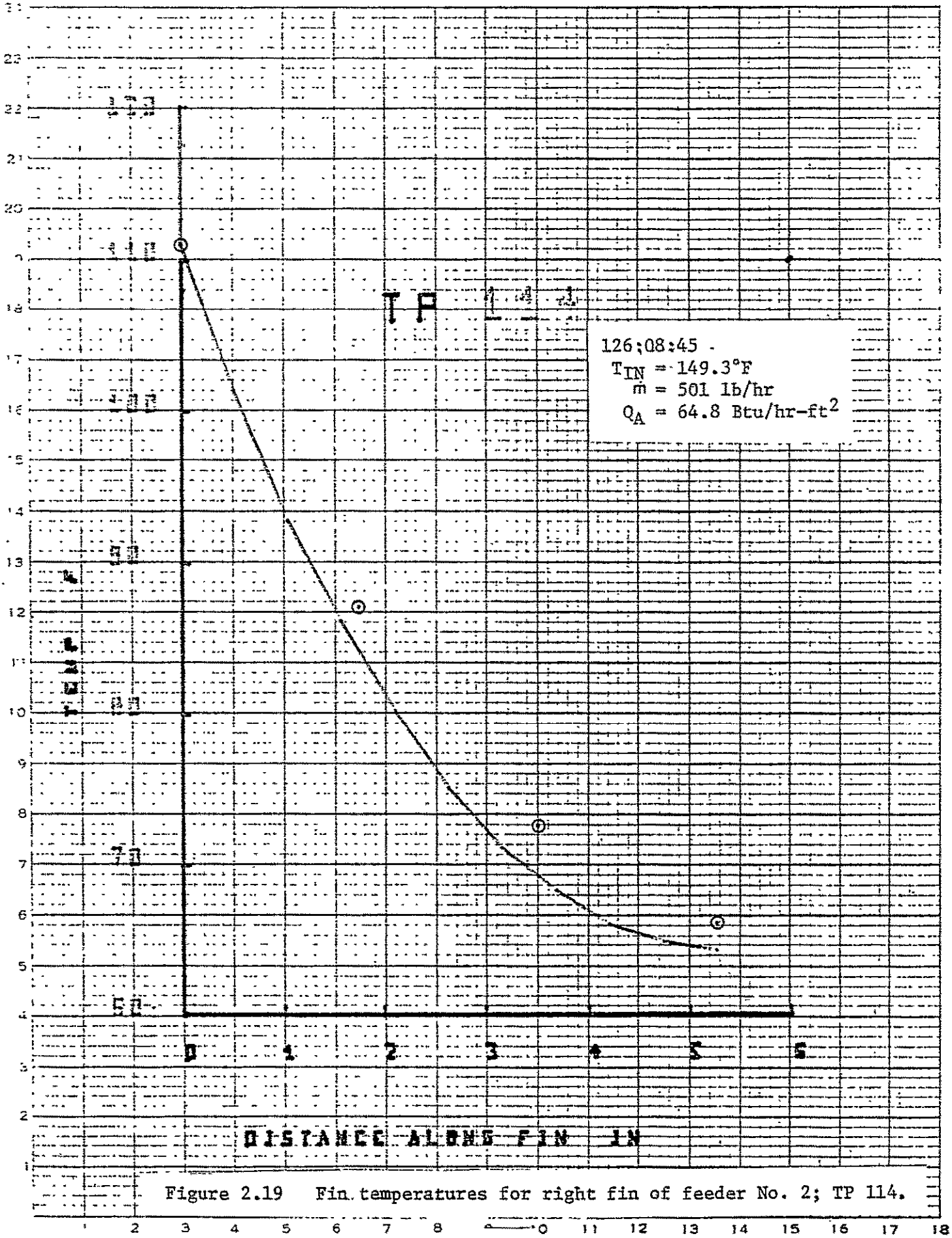

Figure 2.19 Fin temperatures for right fin of feeder No. 2; TP 114.

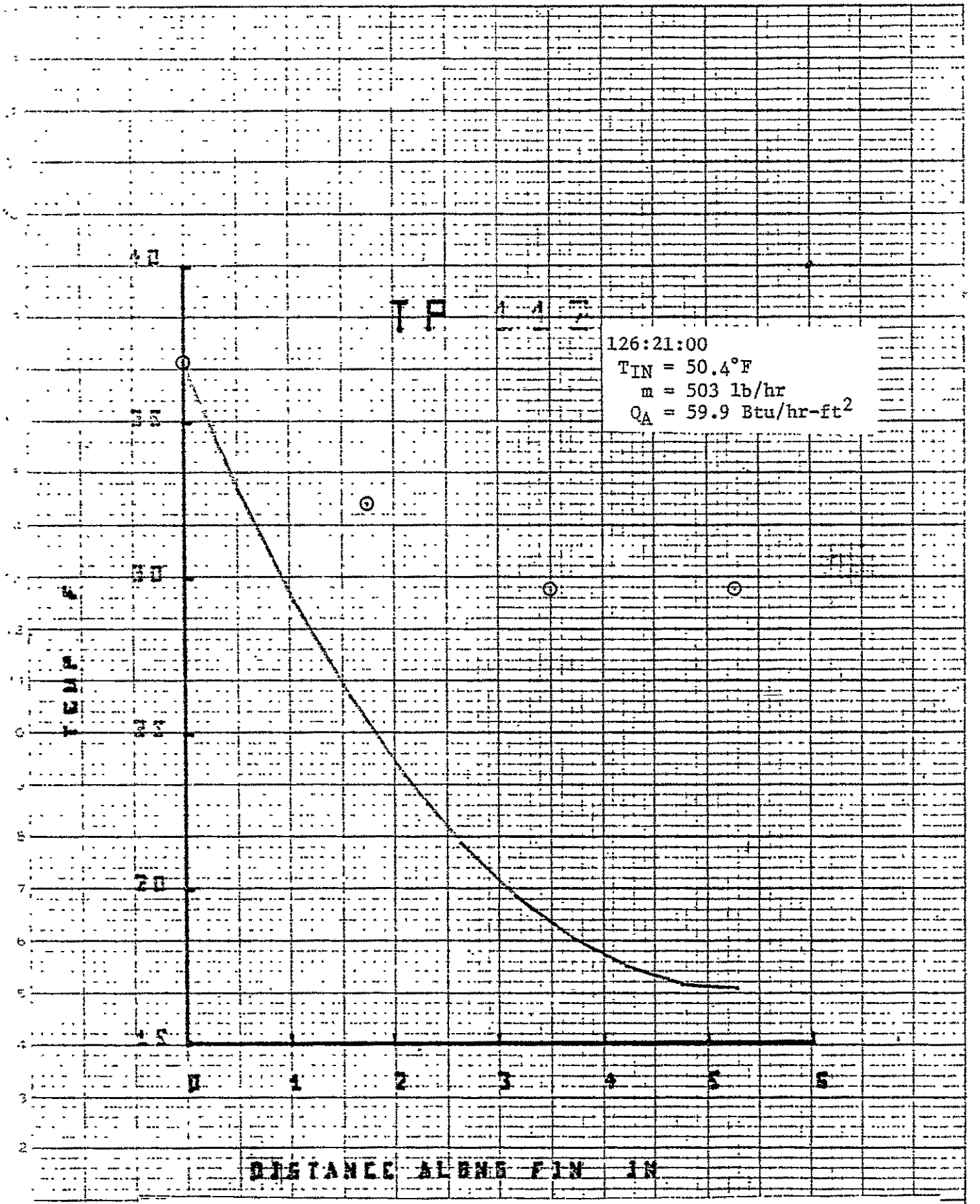

Figure 2.20. Fin temperatures for left fin of feeder No. 7; TP 112.

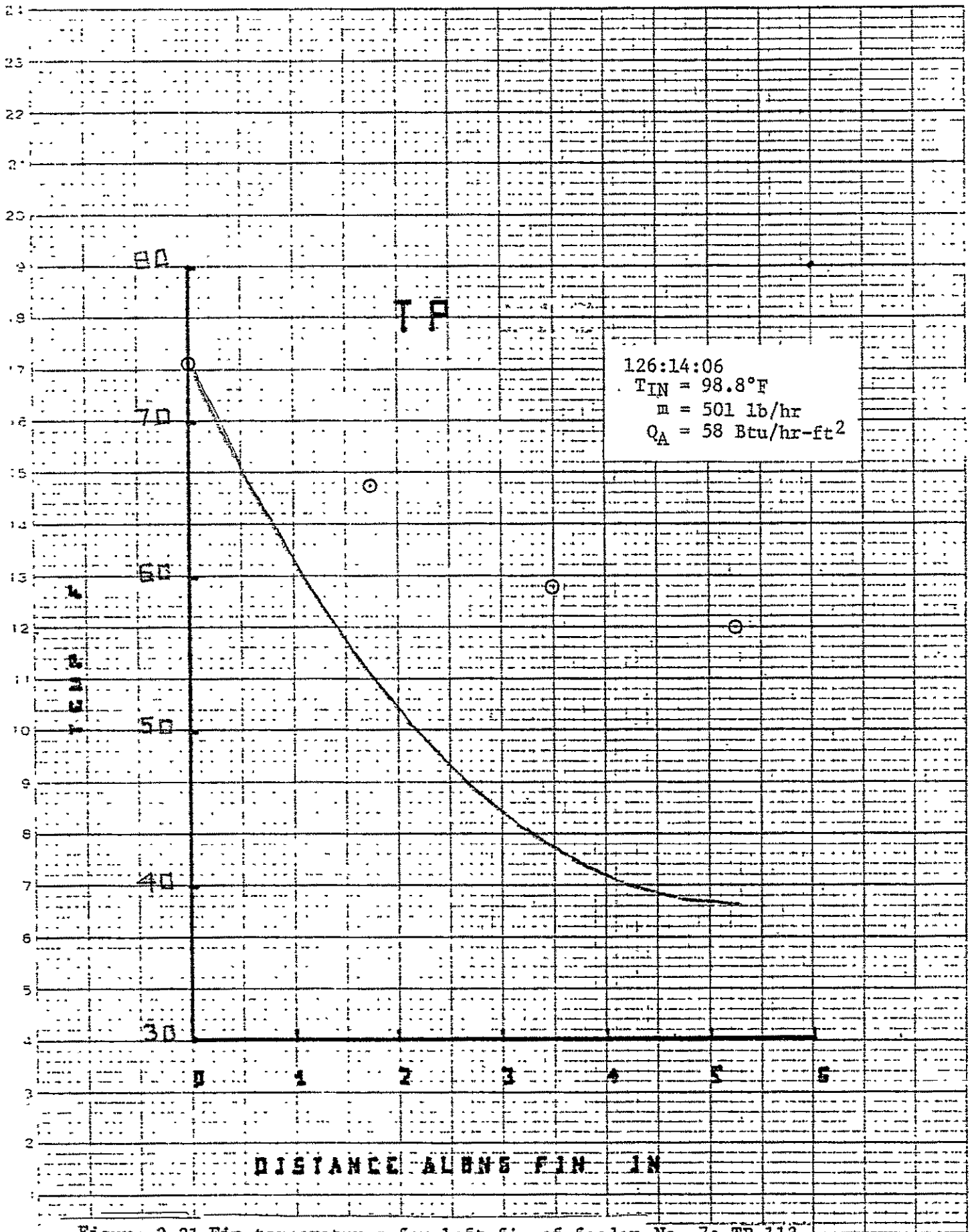

Figure 2.21 Fin temperatures for left fin of feeder No. 7; TP 113.

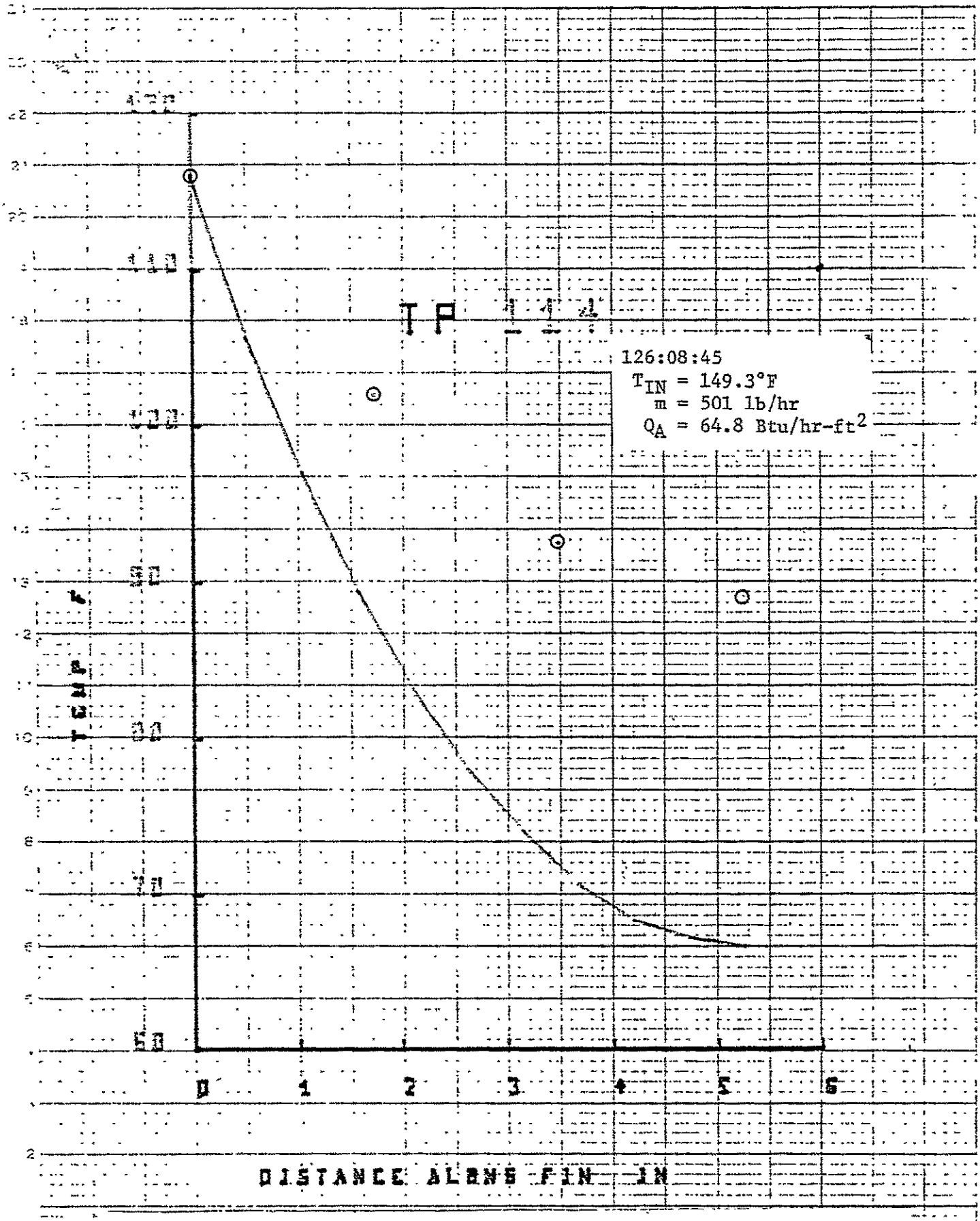

Figure 2.22 . Fin temperatures for left fin of feeder No. 7; TP 114.

perature curve at x = 0 with the experimental heat rejected values. It can be seen, Table 2.5, that again the agreement is reasonable. The calculated heat rejection assumes equal heat transfer to each of the two fins per feeder and the experimental values neglects the heat transfer due to the propane heat pipe.

In another combination of tests (TPs 103, 114 and 123) the heat transfer was increased by decreasing Q_A the absorbed heat flux, Fig. 2.3, all other conditions held constant. The fin-temperature profile comparisons, Figs. 2.23 - 2.26, are similar to that described above except the agreement between calculated and experimental was not so good at the highest environment, Fig. 2.26. In that connection, it should be noted that nonuniformities in the simulator worsened as the environment increased. Again, there was little agreement between the calculated and experimental data for the left fin of feeder No. 7. Comparisons of the heat rejected values are presented in Table 2.5.

A series of tests was made at minimum environments, TPs 127, 128, 129 and 130, where the simulator should have been operating most uniform and best agreement between experimental and calculated fin-temperature distributions could be expected. This was indeed the case, Figs. 2.27 - 2.35. Comparisons of experimental and calculated heat-rejection values, Table 2.5, also indicate good agreement.

TEST PT	FEEDER NO	Q_{CALC} BTU/HR	$Q_{REJ}/11$ BTU/HR
112	2	209	155
	7	215	
113	2	398	295
	7	378	
114	2	504	469
	7	535	
103	2	744	598
	7	641	
123	2	421	346
	7	407	
127	2	463	440
	7	437	
128	2	645	641
	7	615	
129	2	716	749
	7	679	
130	2	807	875
	7	762	

TABLE 2.5. Comparison of calculated heat transfer for feeders No. 2 and 7 with experimental panel total heat rejection divided by eleven.

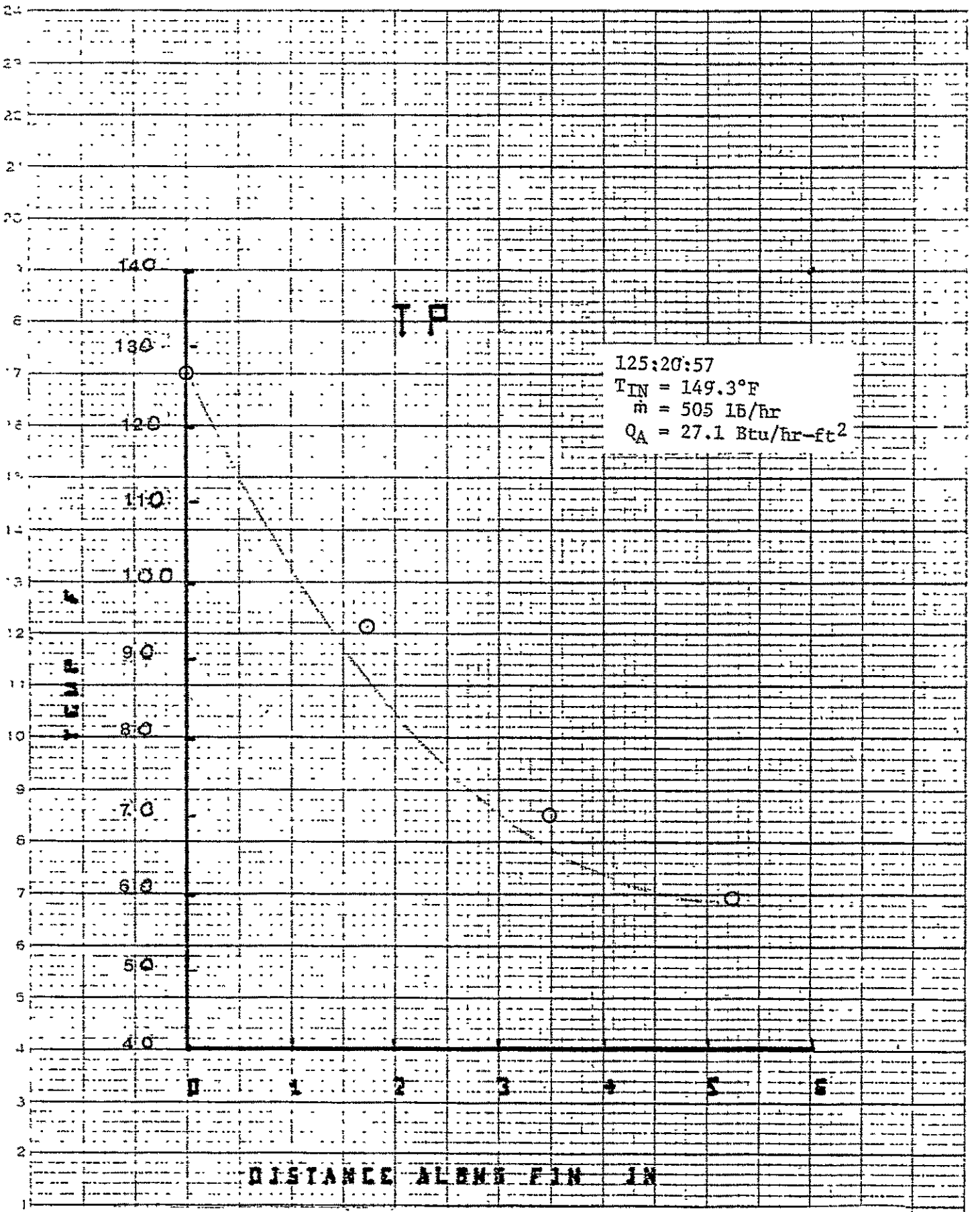

Figure 2.23 Fin temperatures for right fin of feeder No. 2; TP 103.

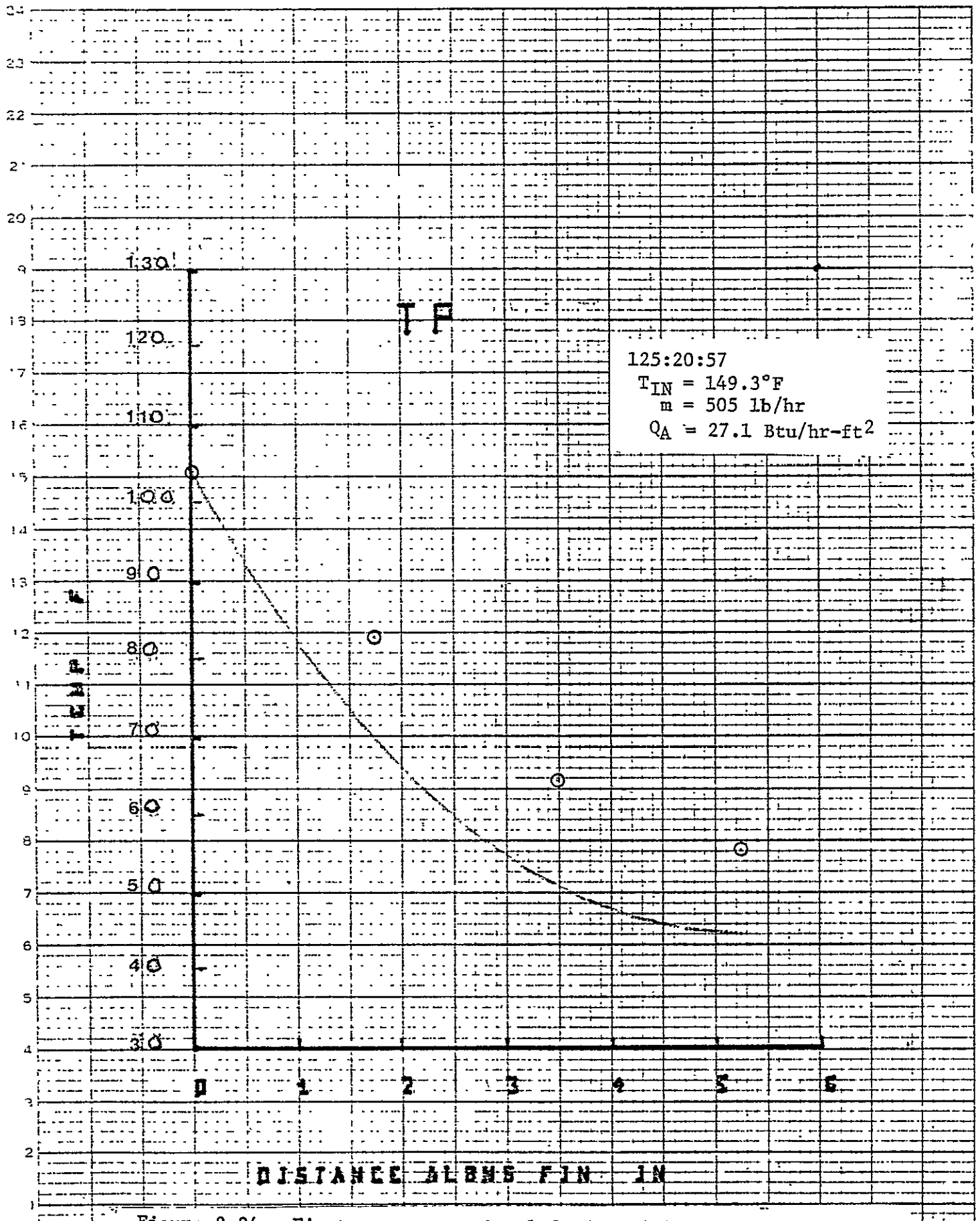

Figure 2.24 Fin temperatures for left fin of feeder No. 7; TP 103.

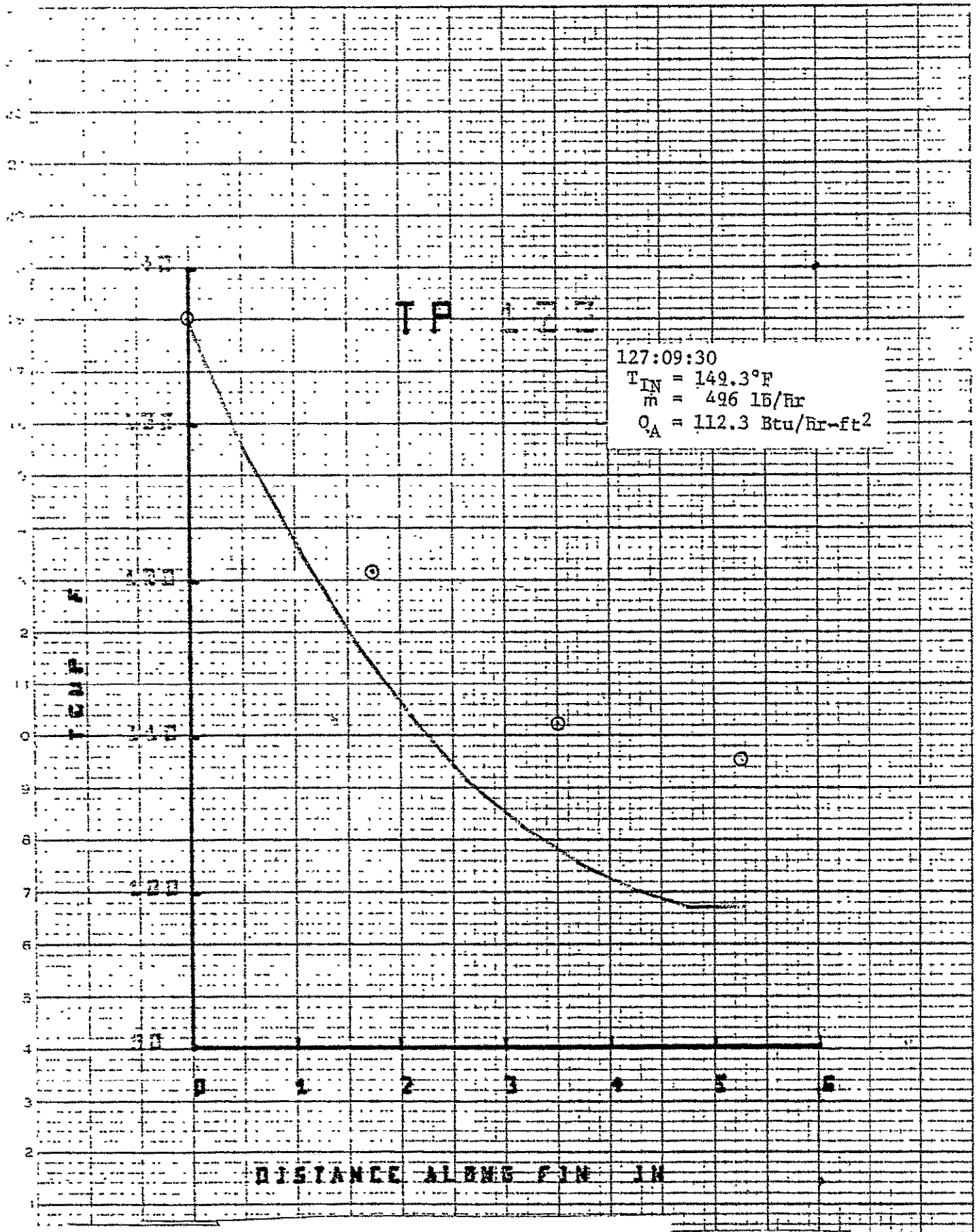

Figure 2.25 Fin temperature for right fin of feeder No. 2; TP 123.

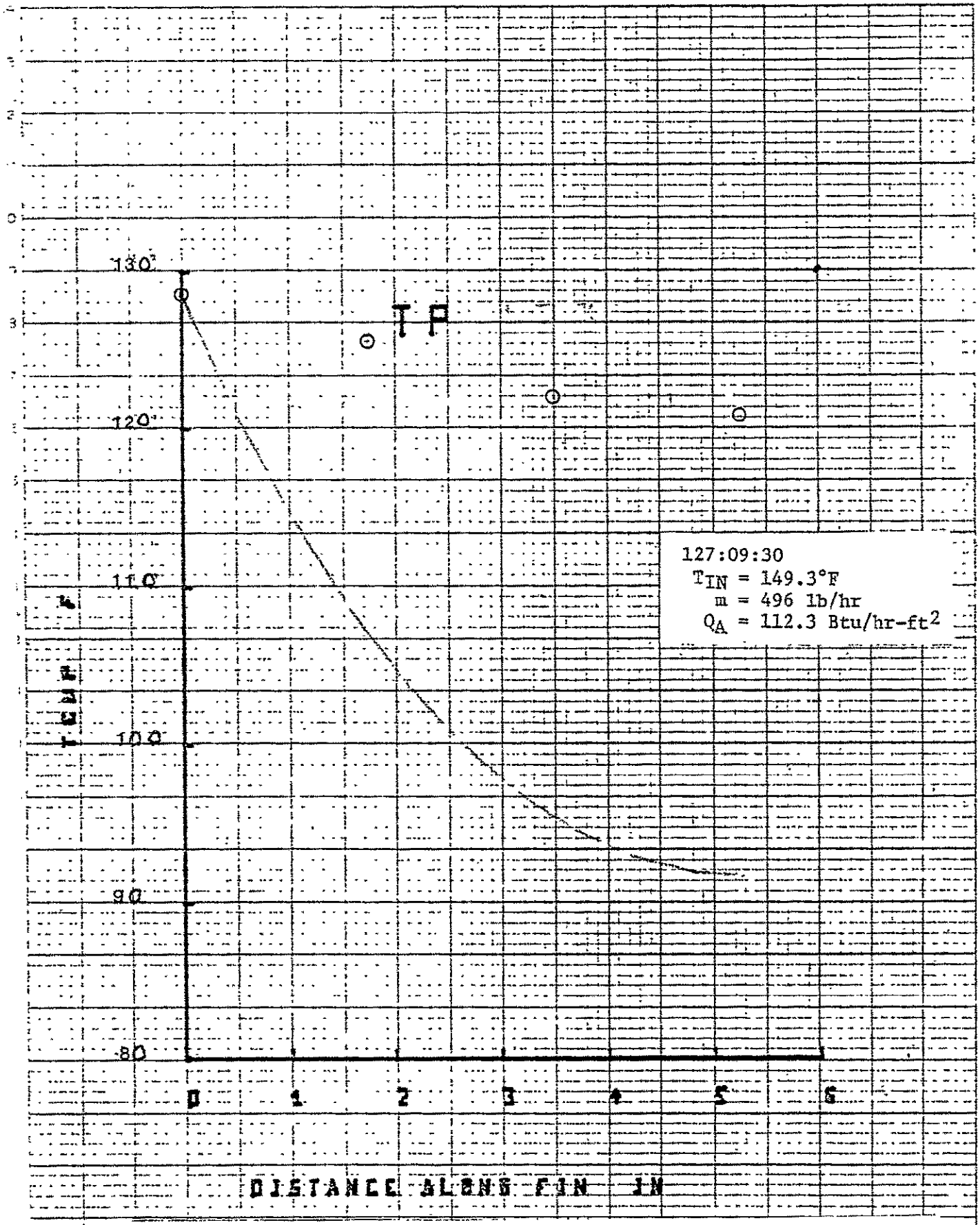

Figure 2.26 Fin temperatures for left fin of feeder No. 7; TP 123.

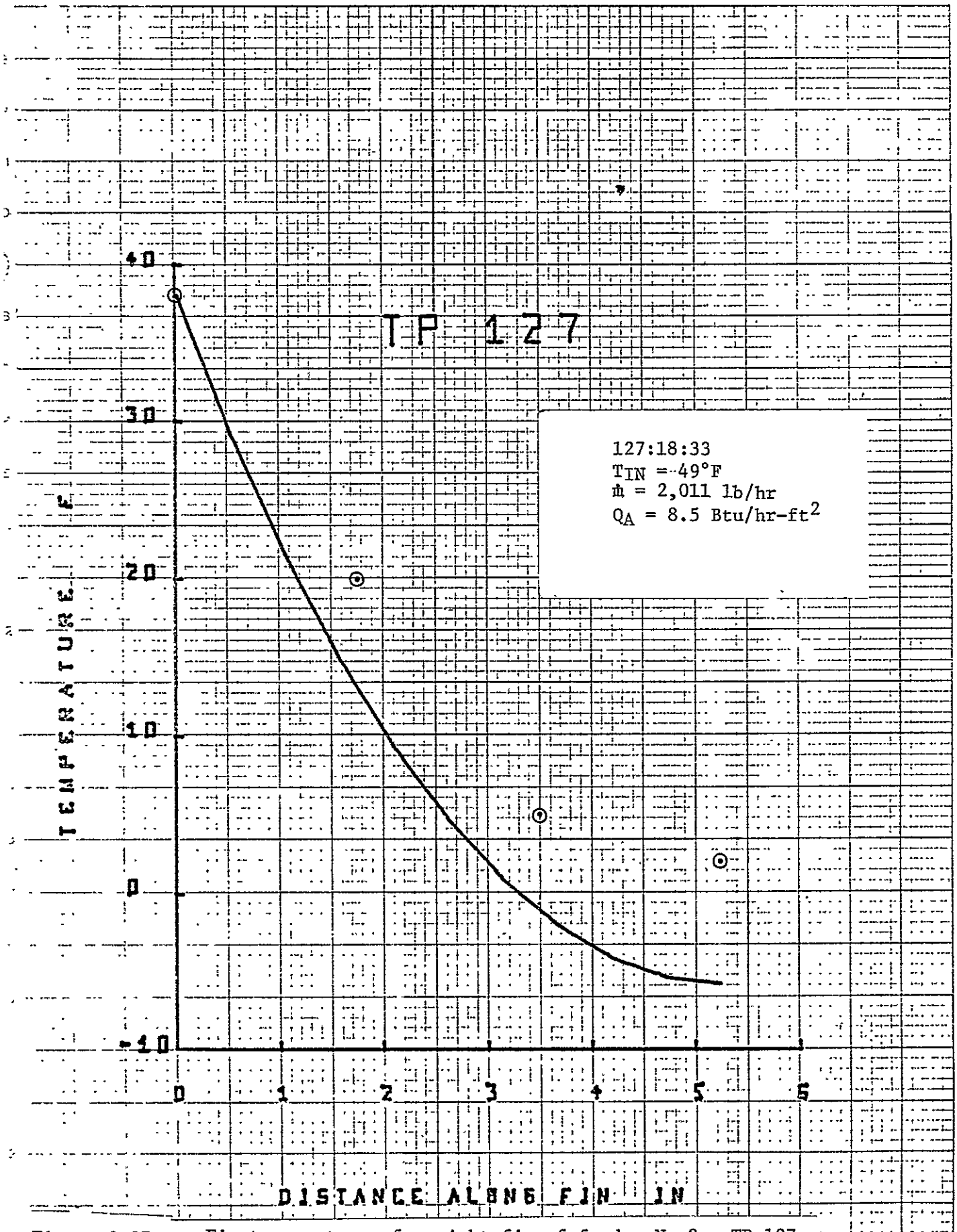

Figure 2.27. Fin temperatures for right fin of feeder No.2; TP 127.

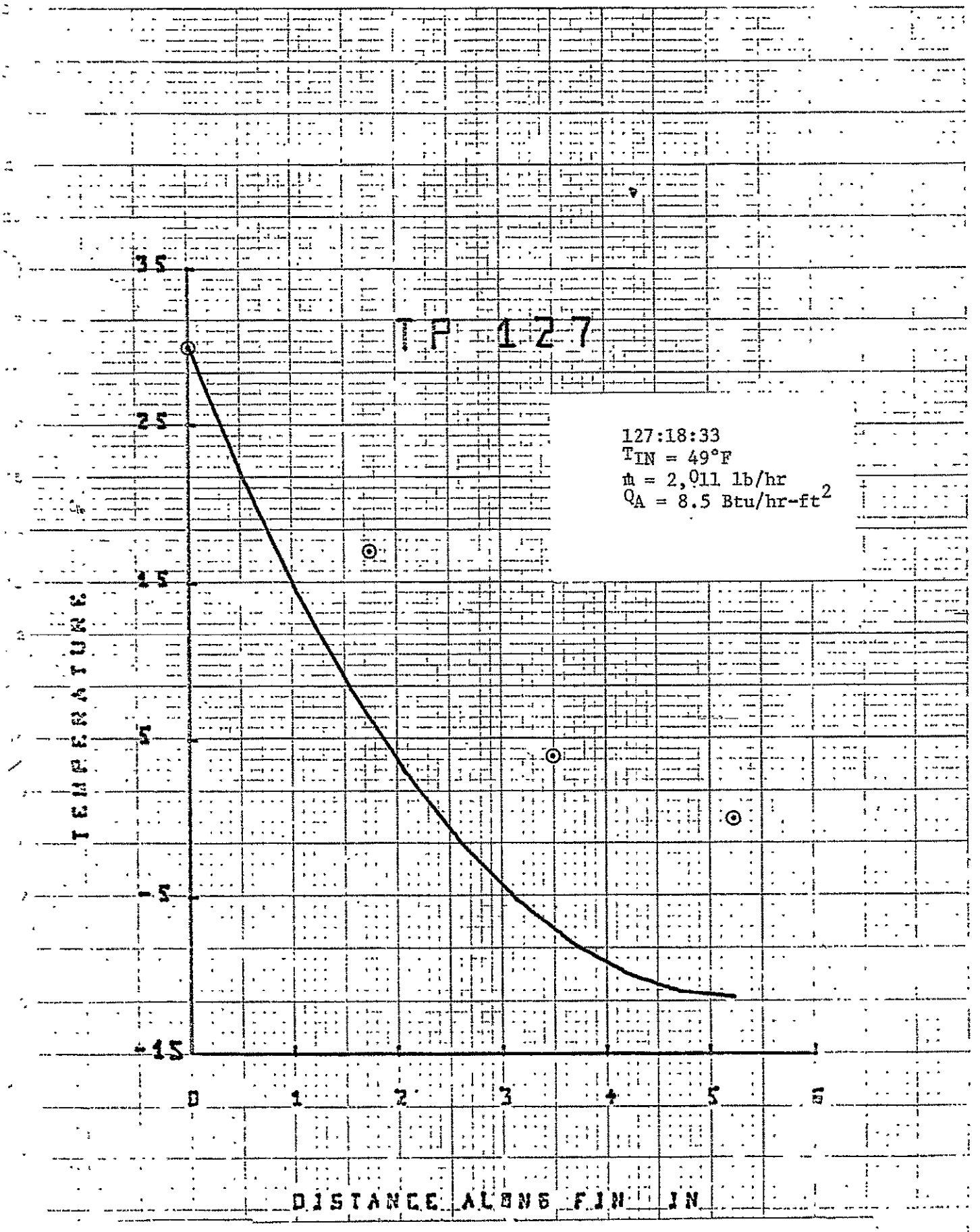

Figure 2.28. Fin temperatures for left fin of feeder No. 7; TP 127.

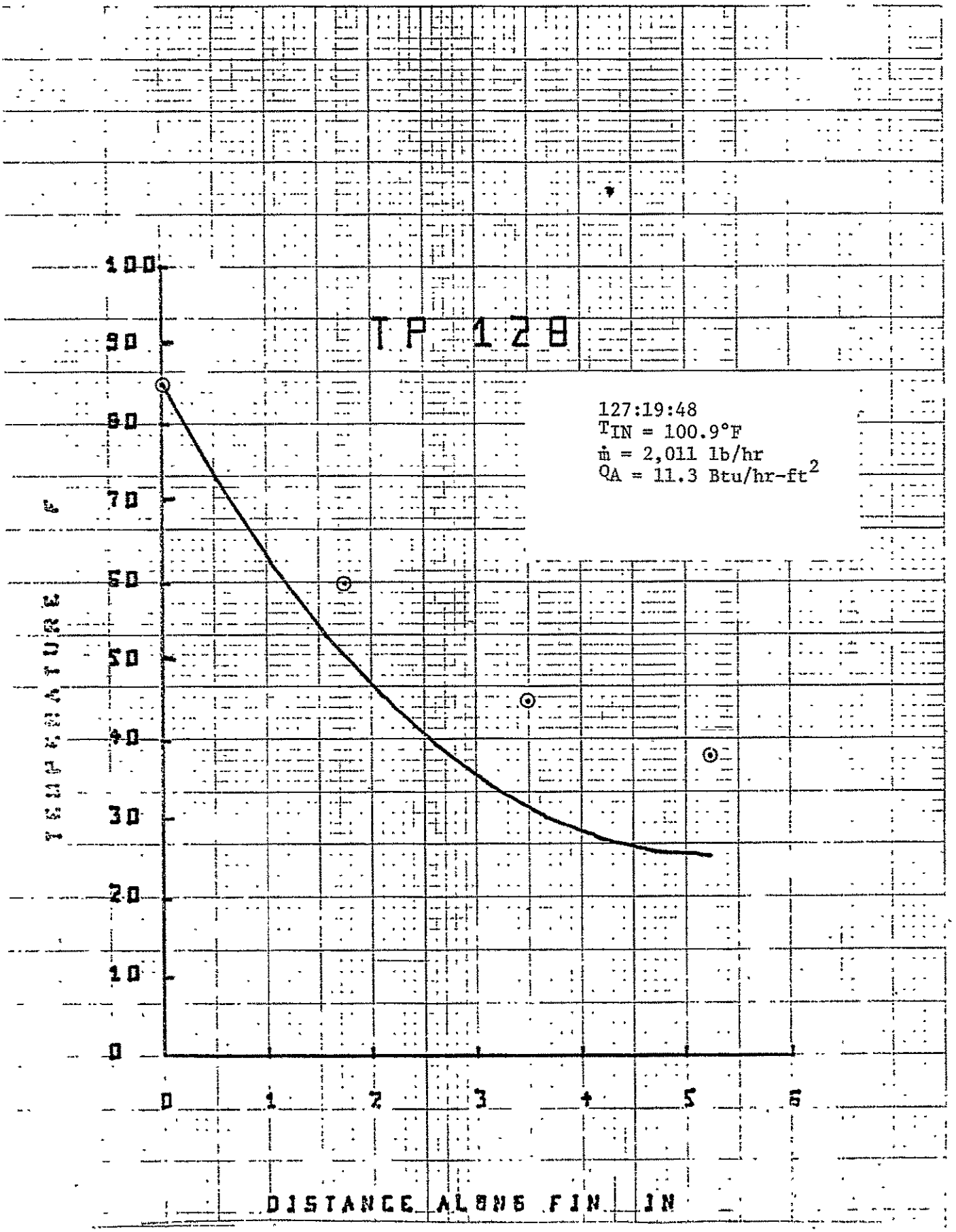

Figure 2.29. Fin temperatures for right fin of feeder No.2; TP 128.

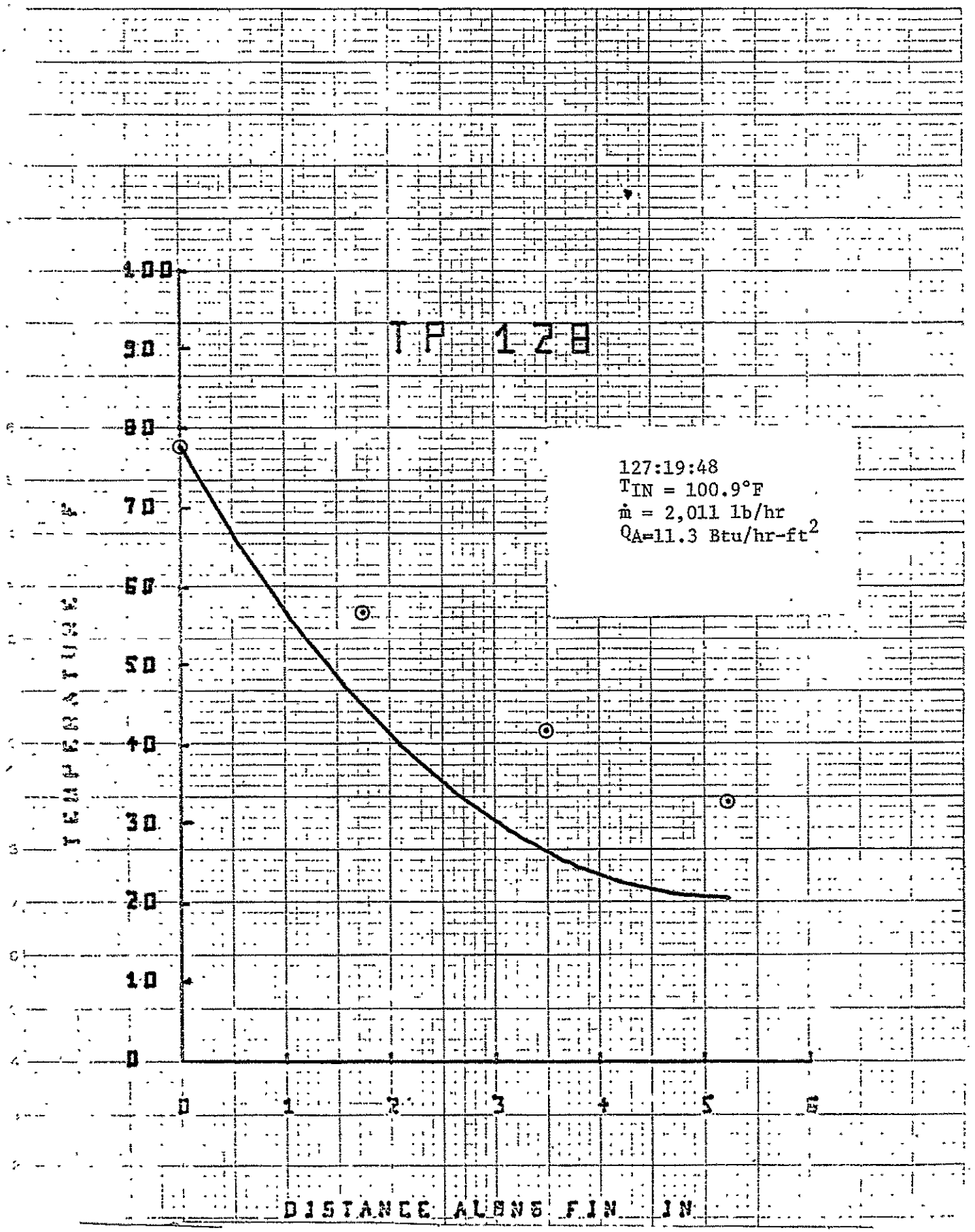

Figure 2.30. Fin temperatures for left fin of feeder No. 7; TP 128.

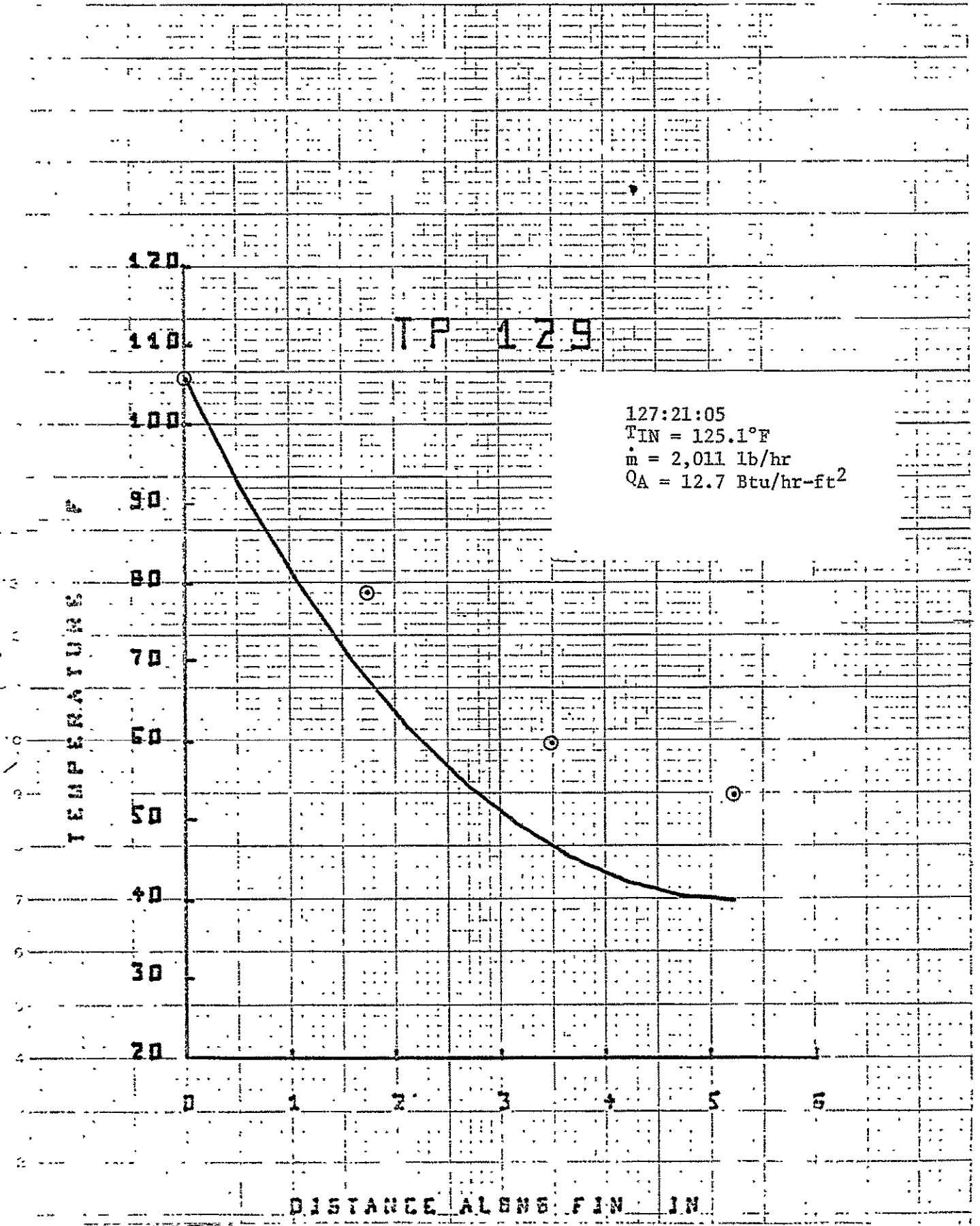

Figure 2.31. Fin temperatures for right fin of feeder No. 2; TP 129.

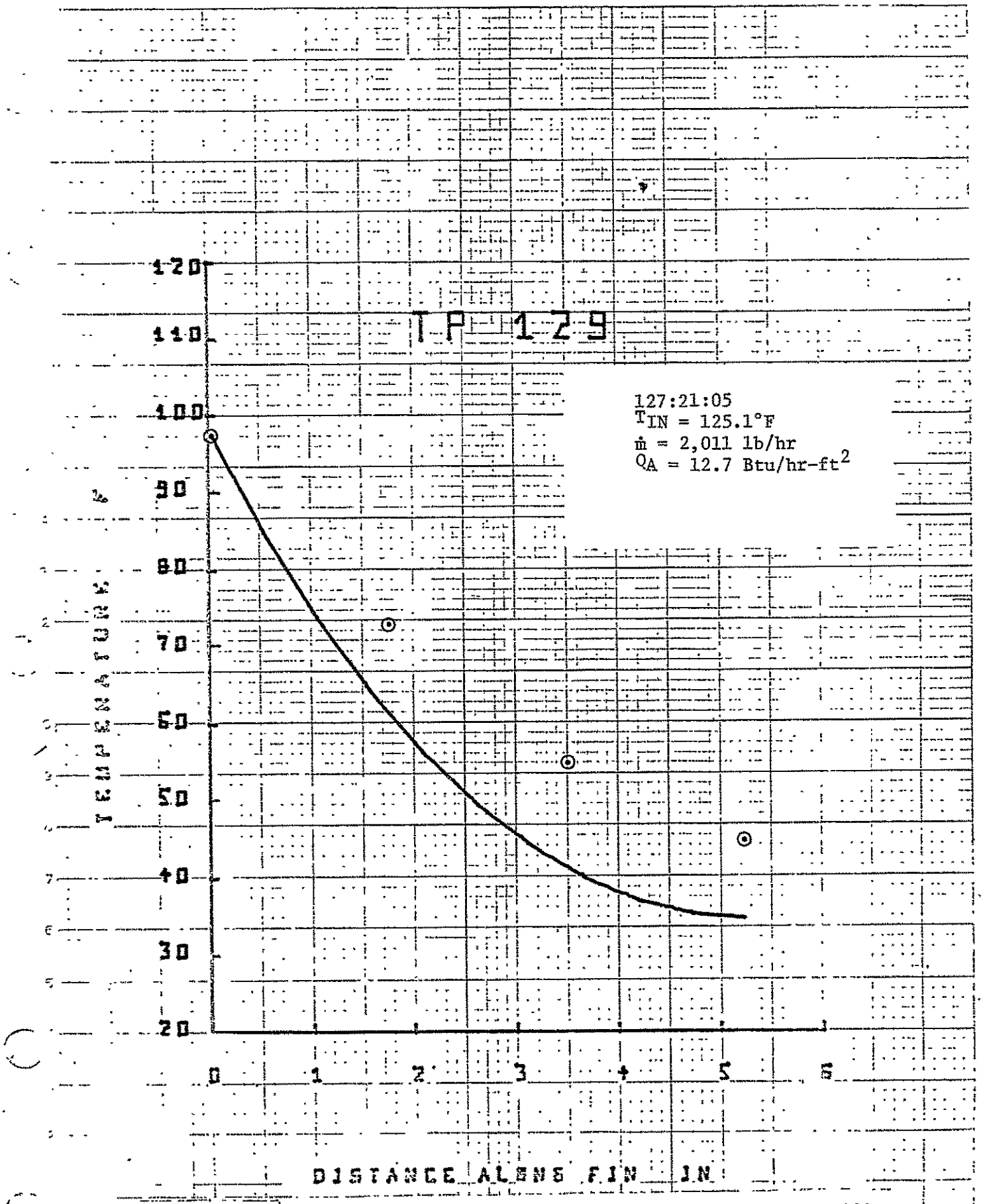

Figure 2.32. Fin temperatures for left fin of feeder No. 7; TP 129.

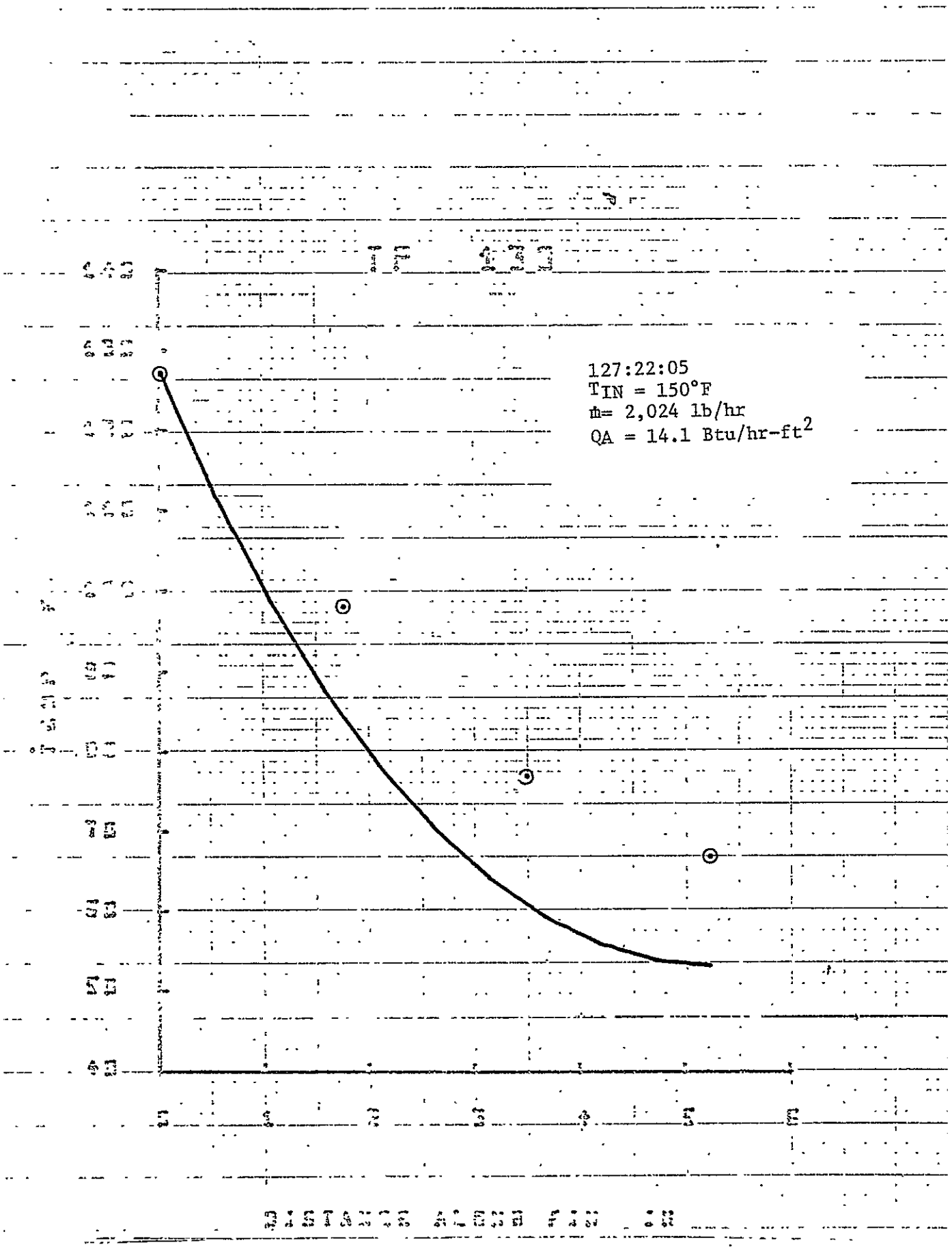

Figure 2.33. Fin temperatures for right fin of feeder No. 2: TP 130.

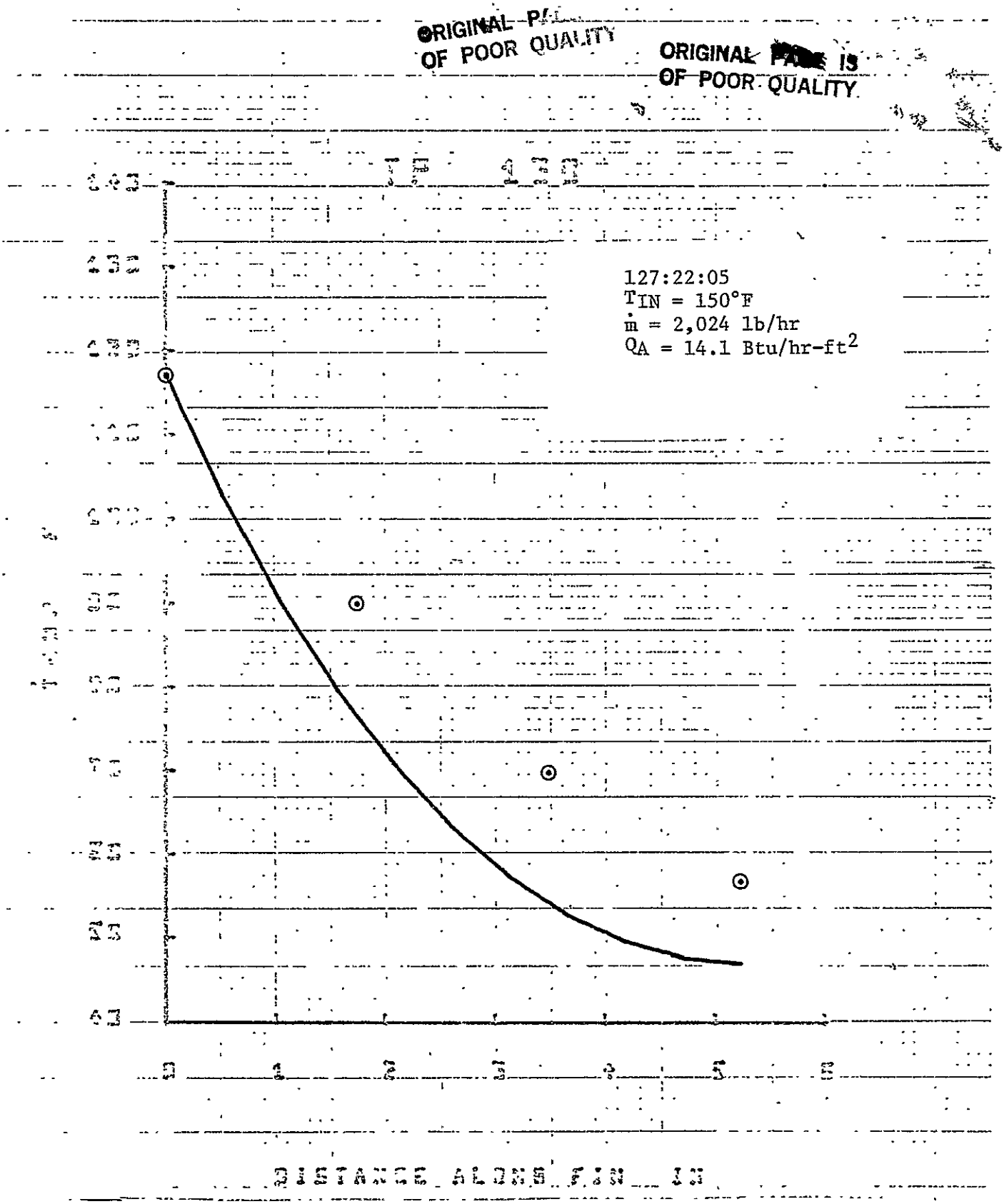

Figure 2.34. Fin temperatures for left fin of feeder No. 7: TP 130.

3. FREEZE-THAW EXPERIMENTS

The three freeze-thaw experiments (TP 209A, 139:19:50; TP 209A, 140:21:00; TP 209A Rep. 142:11:55) made on the prototype panel provided particularly useful information. Freezing of all eleven ammonia heat pipes on the panel was effected by decreasing the flow rate to less than 300 LB/HR and inlet temperature to less than -100° F in the coldest possible environment (Q_A < 10 BTU/HR-FT^2). Under these conditions, the panel froze in about 3 hours.

Thawing of the fluid-header feasibility panel had required over 9 hours (3), considerably longer than the observed fastest time of 45 min for the protytype panel. This large reduction in thaw time which was observed is attributable to the feeder evaporators being placed inside the header for enhanced heat transfer with the coolant fluid rather than welded to the outside wall of the header as they were for the fluid-header feasibility panel.

3.1 Unsuccessful thaw attempt at time 139:19:50 (TP 209A)

The thaw attempt at time 139:19:50 was interesting although in a negative manner, since an inadvertent rapid rise in the header inlet temperature from -140° F to 40° F and flow from 0 to 500 LB/HR in minutes occurred, Fig. 3.1, and the panel failed to thaw. The thermal shock which resulted from such a rapid increase in source temperature inactivated the propane heat pipe, Fig. 3.2. From a study of data similar to Fig. 3.1, it was concluded that the shock also set-up prohibitively high heat-loads on the feeder evaporators, since they did not heat pipe after thawing.

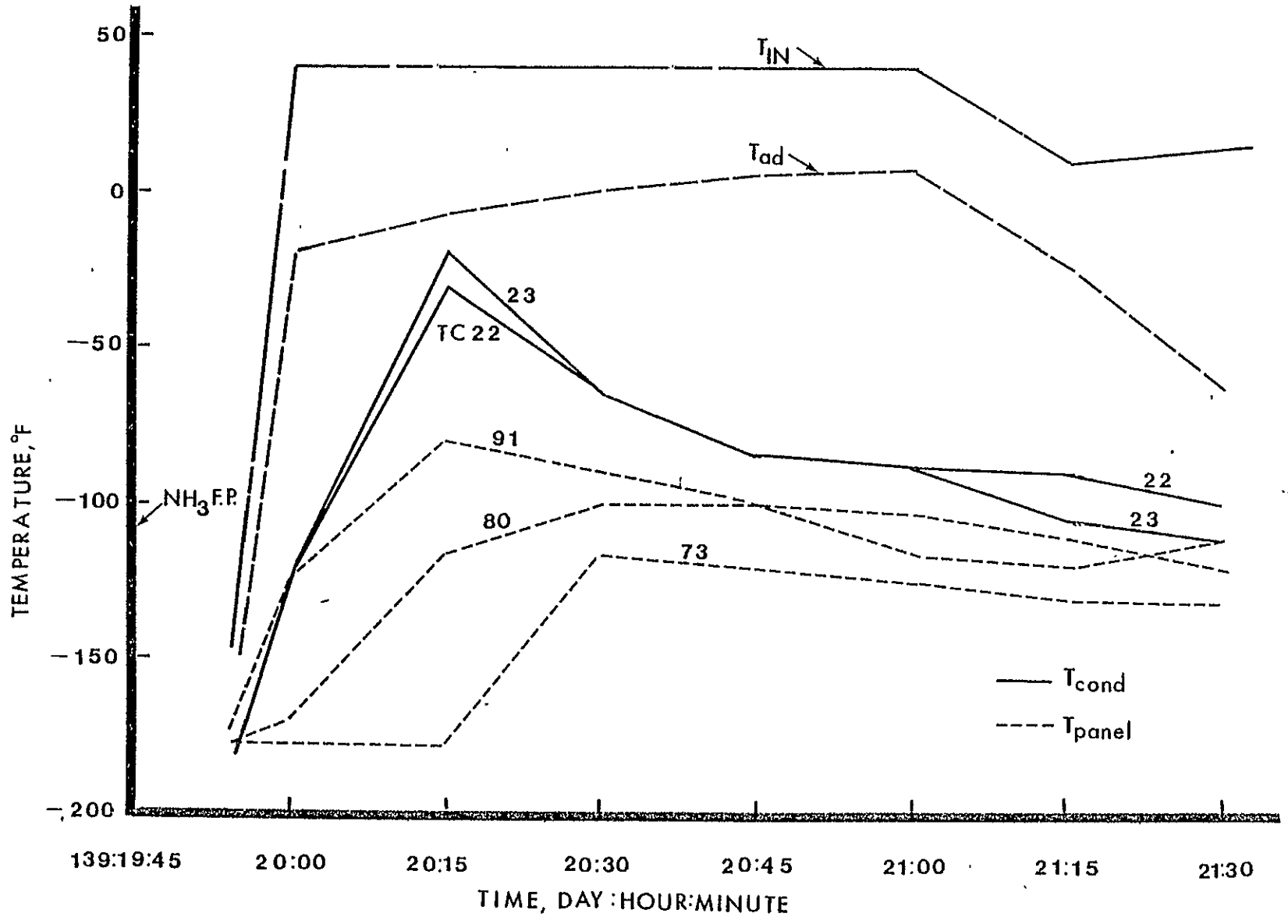

P. 3-47
PRECEDING PAGE BLANK-NOT FILMED

Figure 3.1 Temperatures vs time for feeder No. 2 showing failure to go into heat pipe mode after thaw.

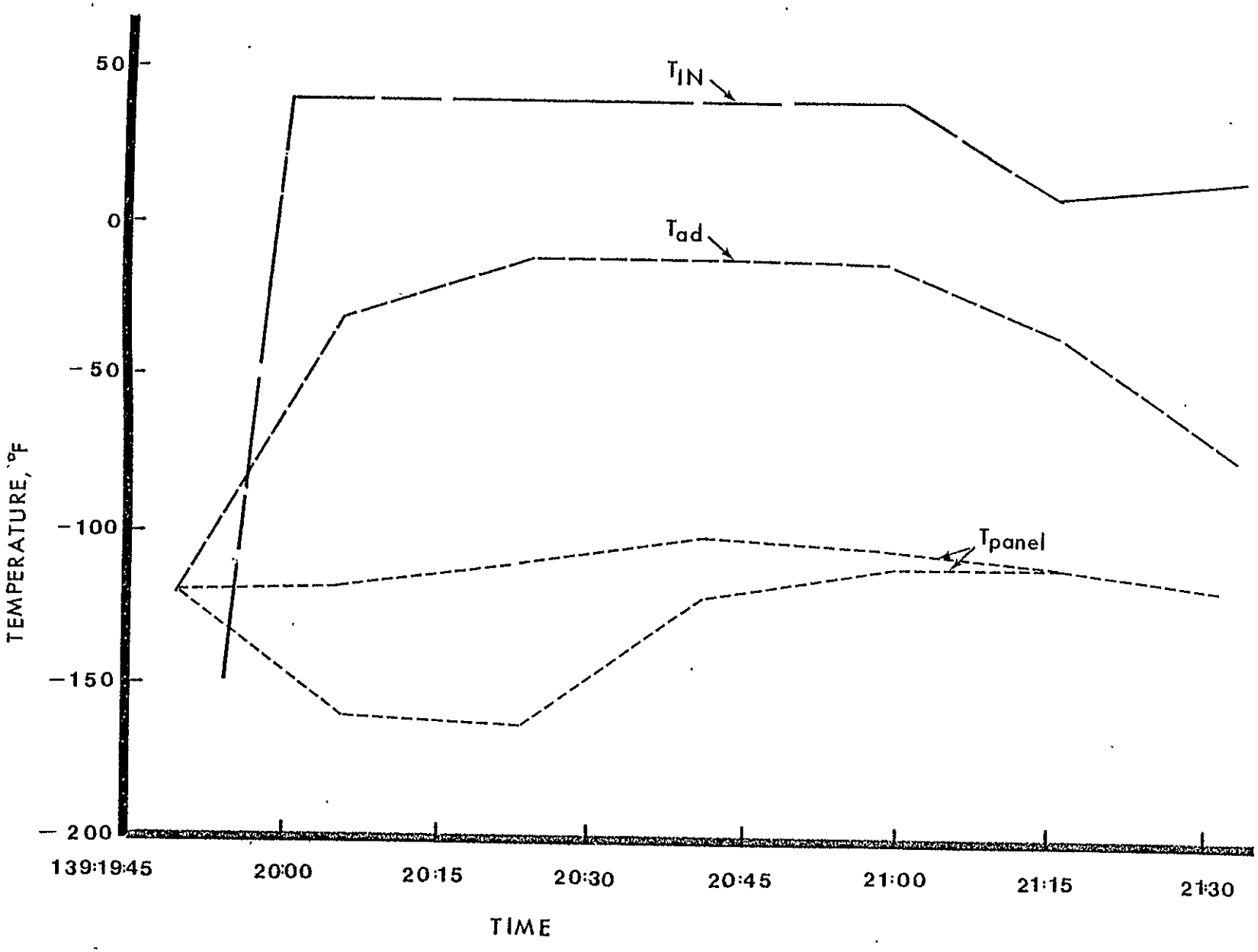

Figure 3.2. Propane heat pipe temperatures during unsuccessful thaw attempt at time 139:19:50.

3.2 Freeze-thaw attempts at times 140:21:00 (TP 209B) and 142:11:50 (TP 209A Rep.)

During the two subsequent thaw experiments, TP 209B and TP 209A Rep, however, the planned rate of increase of header fluid inlet temperature, approximately 2° F/min, $\dot{m} \approx 500$ LB/HR, was supplied and for TP 209A Rep the panel thawed rapidly reaching normal heat rejection in about 3 hours, Fig. 3.3a. The elapsed time from beginning of thaw to the heat-pipe mode was about 45 min., Fig. 3.4. A study of the limited feeder heat-pipe condenser tube temperatures (measured on feeder heat pipes Nos. 2, 7, and 12), Figs. 3.4, 3.5 and 3.6, and the panel temperatures that were taken indicated that these three feeders recovered from the freeze nearly simultaneously, and consequently, the propane heat pipe had negligible influence on the panel thaw. Note also that most of the panel temperatures at a given time during the freeze-recovery sequence were lower than the heat-pipe condenser tube temperatures, Figs. 3.4, 3.5 and 3.6. Thus, the temperature data for TP 209A Rep clearly indicate that the major heat-transfer contributions for the freeze-thaw recovery come from inside the heat pipes plus conduction through the tube walls rather than from heat conduction through the radiator fins.

Somewhat different thawing results were obtained for TP 209B. A comparison, Fig. 3.7, of the feeder adiabatic temperatures (a tube-wall thermocouple on the short transport section located between the evaporator and the condenser) for TP 209A Rep and TP 209B shows, however, that the adiabatic temperature rise as a result of the increase of T_{IN} are similar. The adiabatic temperature is believed important as it approximates closely the feeder vapor temperature, and it can be seen that in both tests a time period of about 1 hour from the beginning of

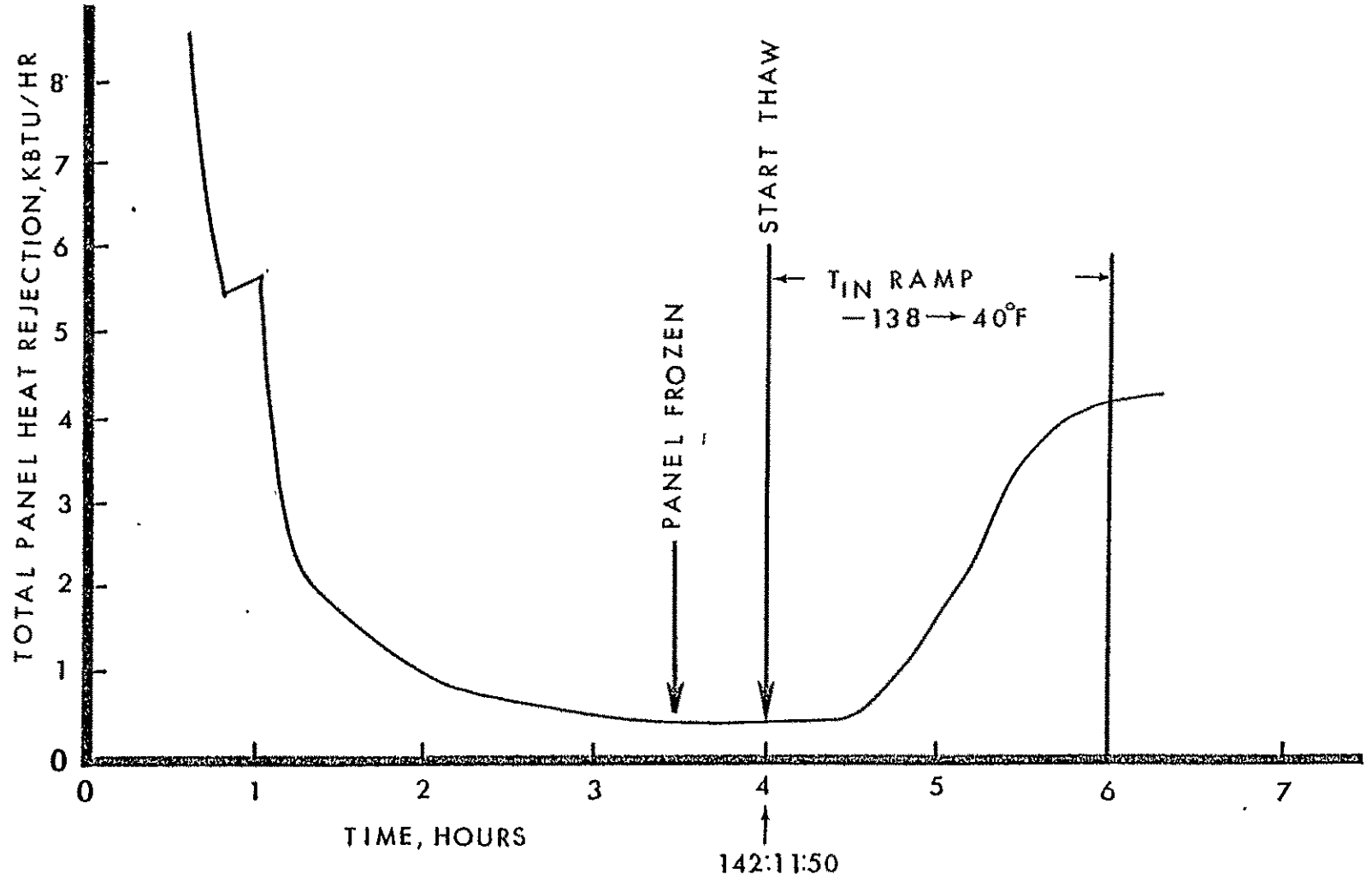

Figure 3.3a. Radiator freeze-thaw performance: TP 209A Rep.

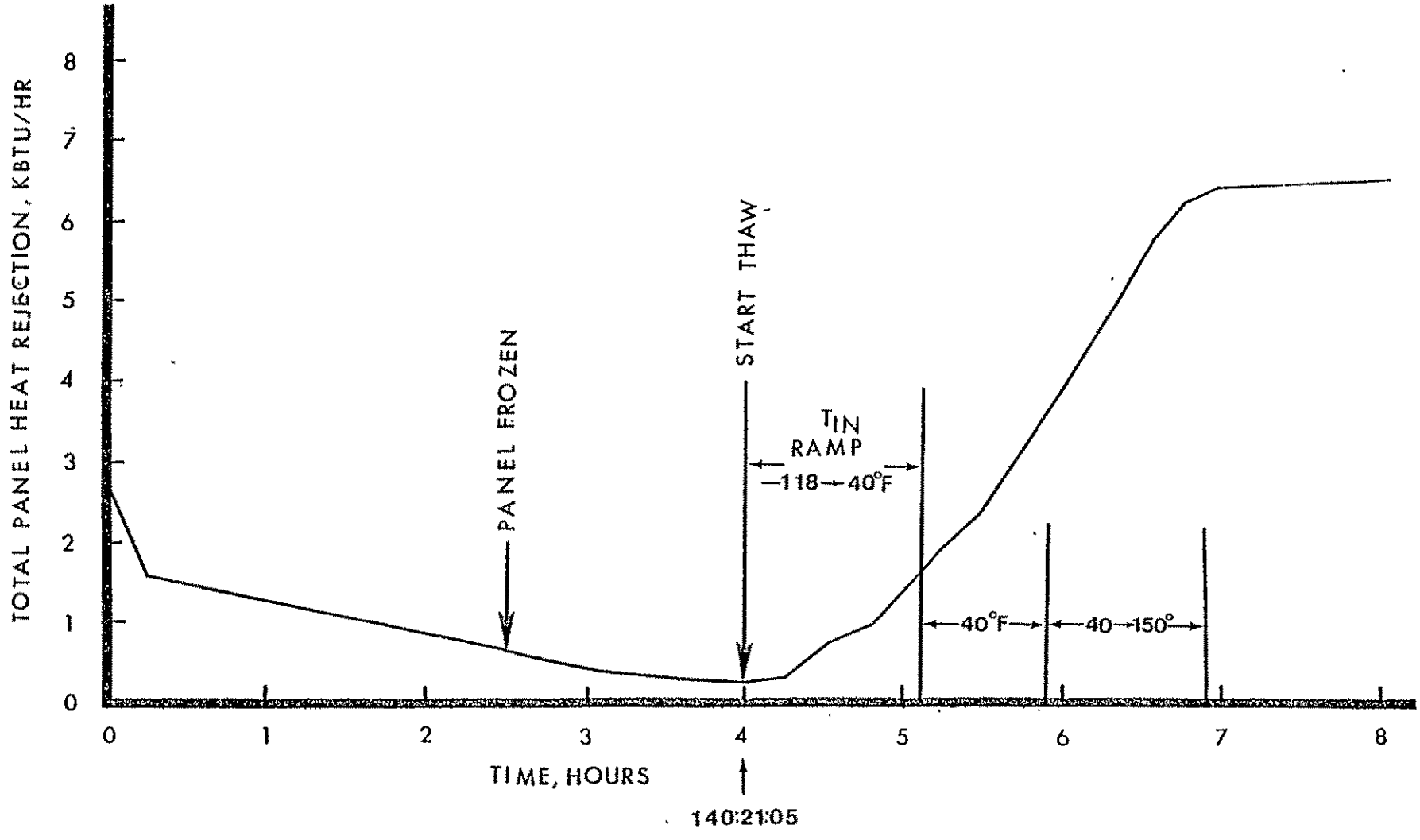

Figure 3.3b. Radiator freeze-thaw performance; TP 209B.

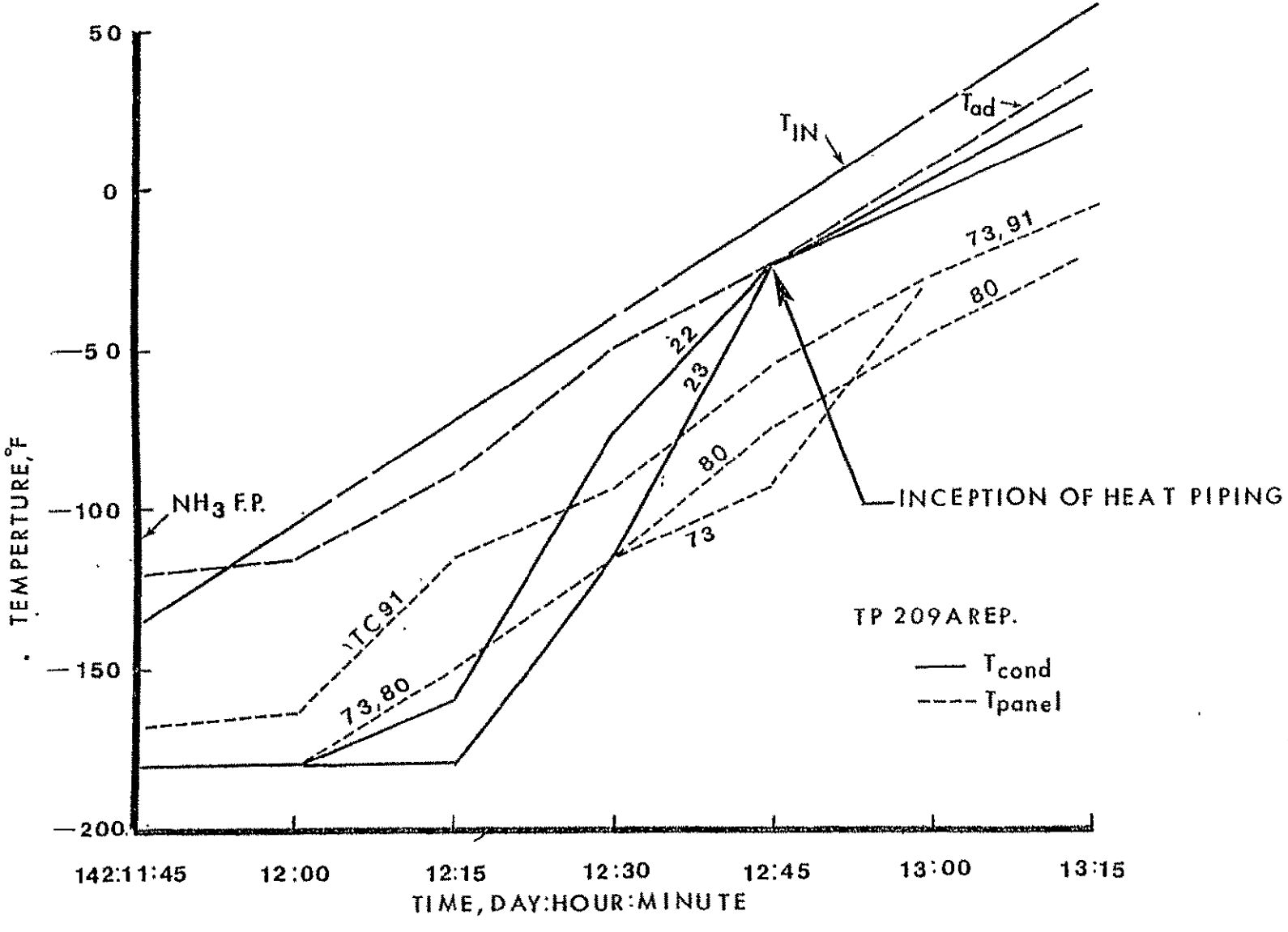

Figure 3.4 Temperatures vs time for feeder No. 2 showing successful heat-pipe recovery after thawing.

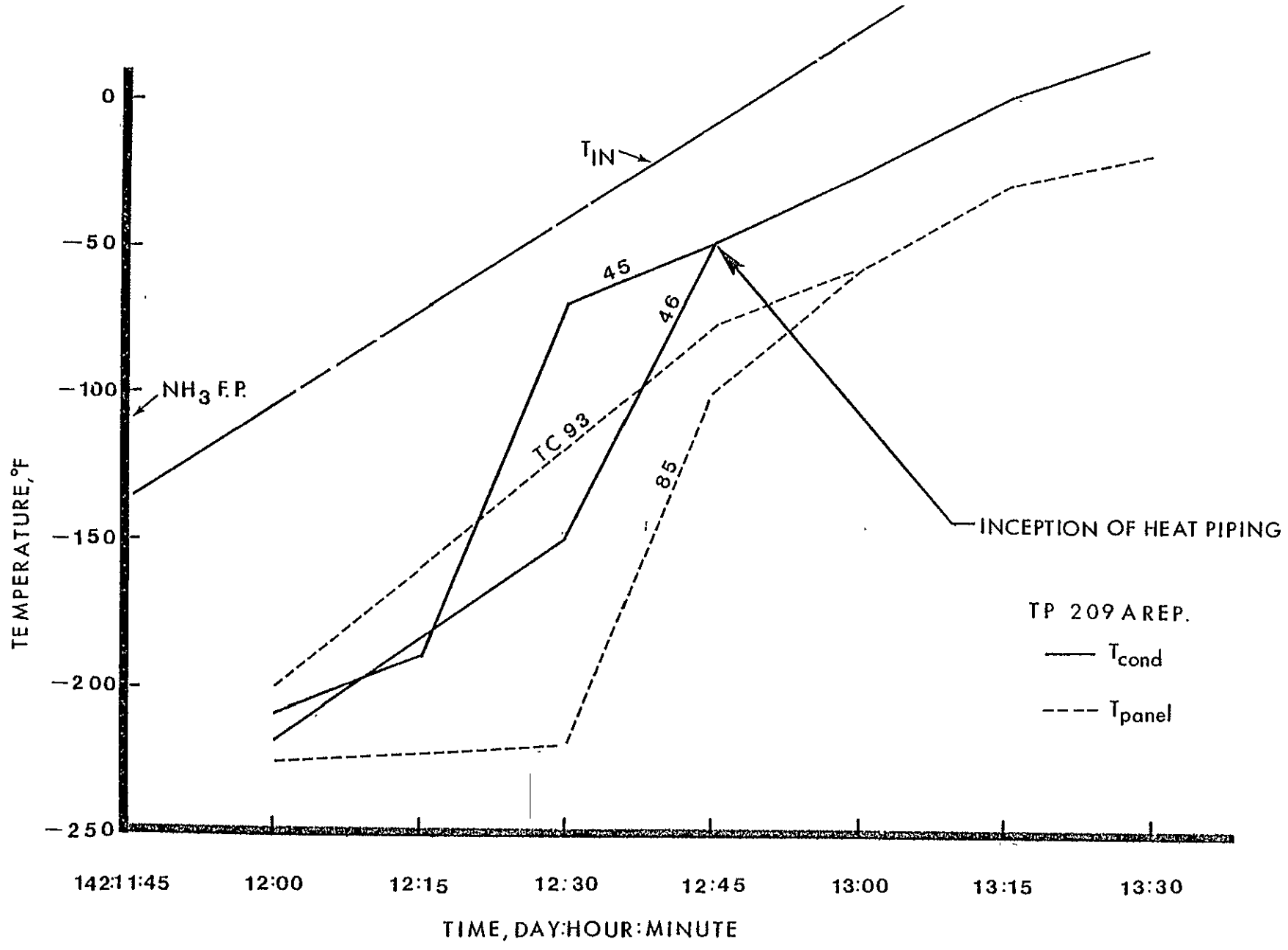

Figure 3.5 Temperatures vs time for feeder No. 7 showing successful heat-pipe recovery after thawing.

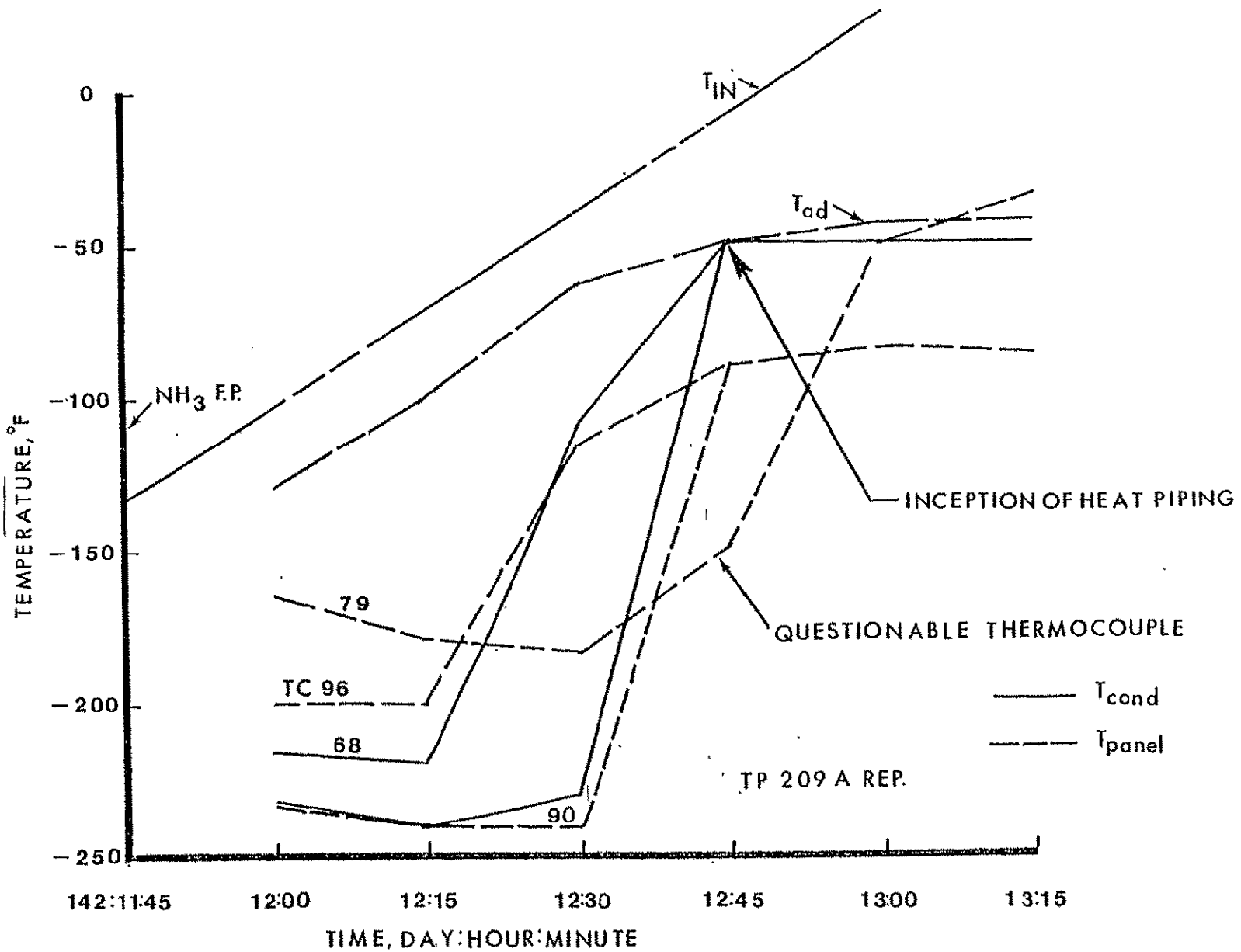

Figure 3.6 Temperatures vs time for feeder No. 12 showing successful heat-pipe recovery after thawing.

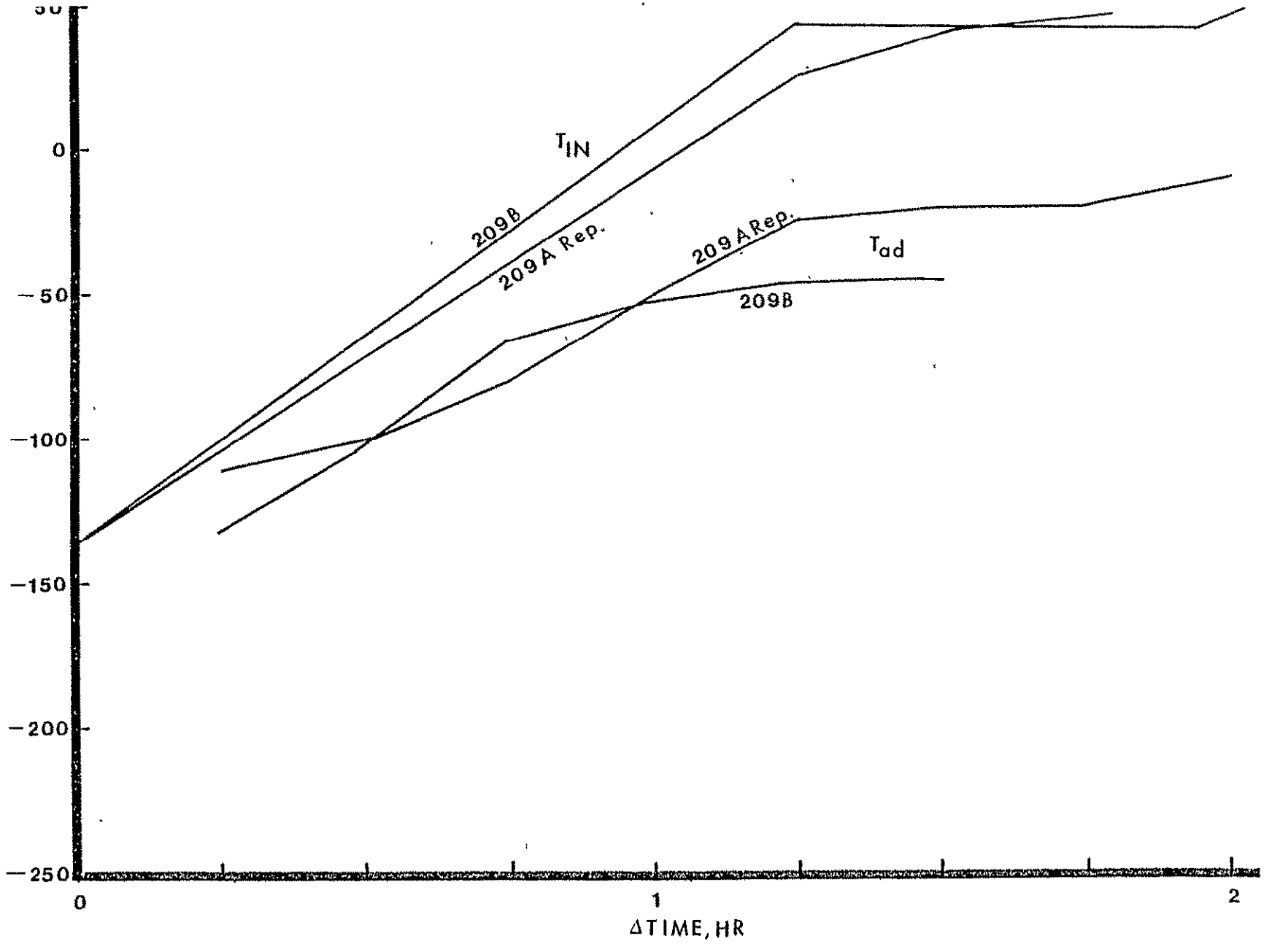

Figure 3.7 | Comparison of T_{ad} ($\simeq T_V$) for feeder No. 12 during thaws of Test Points 209B and 209A Rep.

the thaw was required for the adiabatic temperature of heat pipe No. 12 to increase to -50° F. At this temperature level the existence of liquid ammonia in the evaporator and adiabatic sections was assured. In both tests, therefore, the potential for thawing and heat piping existed after 1 hour into the thaw. The freon flow for the two test points* was about 500 LB/HR.

In Fig. 3.8, the temperatures of No. 12 feeder condenser at two locations during the thaws are presented. Now, unlike the adiabatic temperatures, a significant difference in the thawing characteristics of feeder No. 12 condenser between the two test points is clearly evident: In TP 209A Rep. thawing and heat piping of feeder No. 12 occurred rapidly as mentioned above, but during TP 209B after two hours the condenser had not thawed! Feeder No. 11 during TP 209B also did not thaw, as indicated by the low panel temperature (< 109° F). Condenser thermocouples were not installed on feeder No. 11 but were installed on feeder No. 7, consequently, a good comparison between the thaws of the two test points is again possible. The data, Fig. 3.9, show that the thaw of feeder No. 7 was slower during TP 209B, although feeder No. 7 differences are not nearly as pronounced as those for feeder No. 12. During TP 209A Rep., feeder No. 7 condenser temperatures increased rapidly to about -50° F with no lag at the NH_3 freezing point (-109° F). During TP 209B the feeder No. 7 condenser temperatures initially rose rapidly to -109° F, but remained at that level for nearly 15 minutes before resuming

---

*The data print-out indicates zero flow at times 140:21:00 to 140:22:15 due to a flow cart malfunction which required using a different flow meter. According to the log book the flow was about 500 LB/HR, essentially the same as in TP 209A Rep.

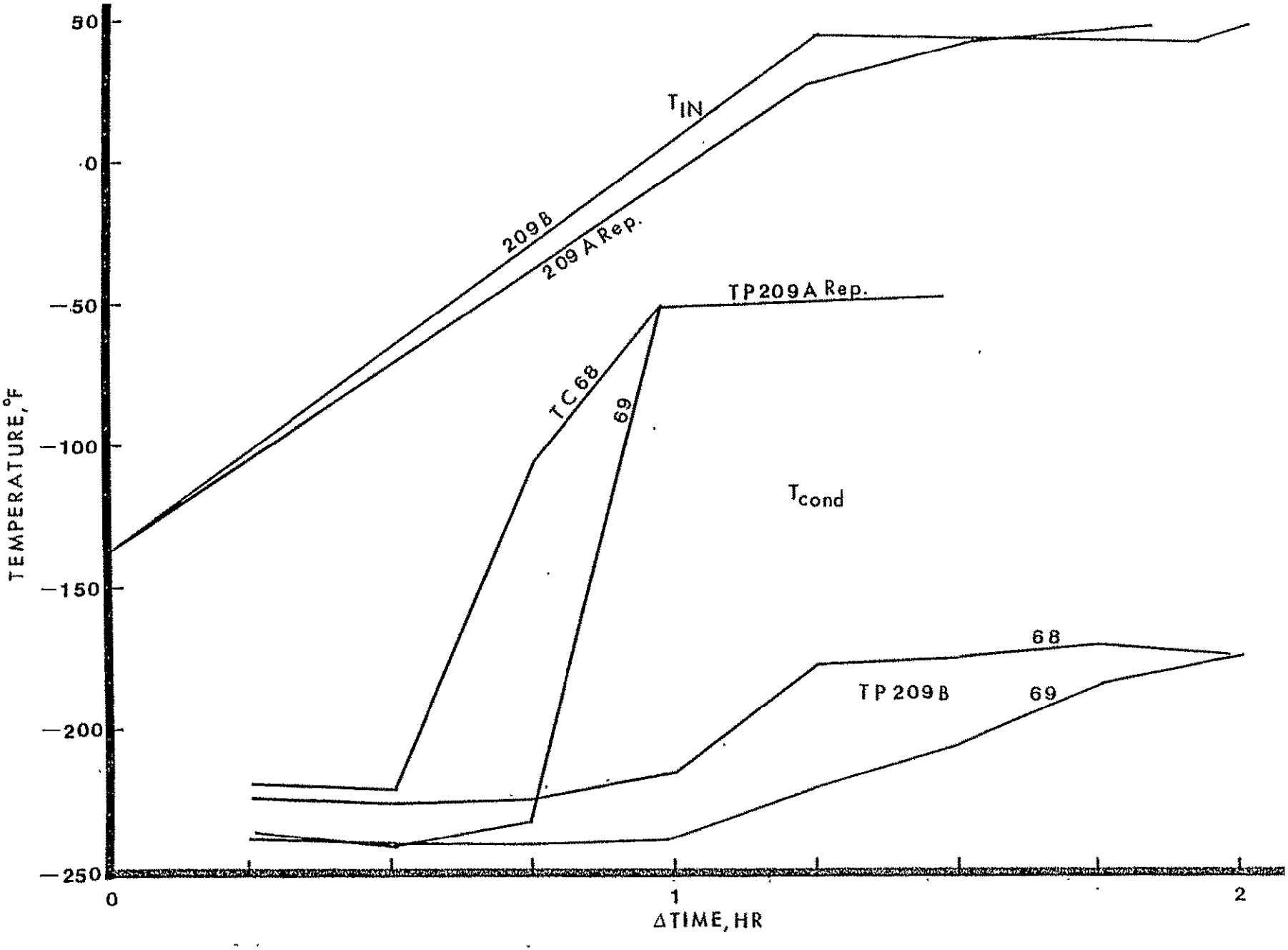

Figure 3.8 Comparison of T_{cond} for feeder No. 12 during thaws of Test Points 209B and 209A Rep.

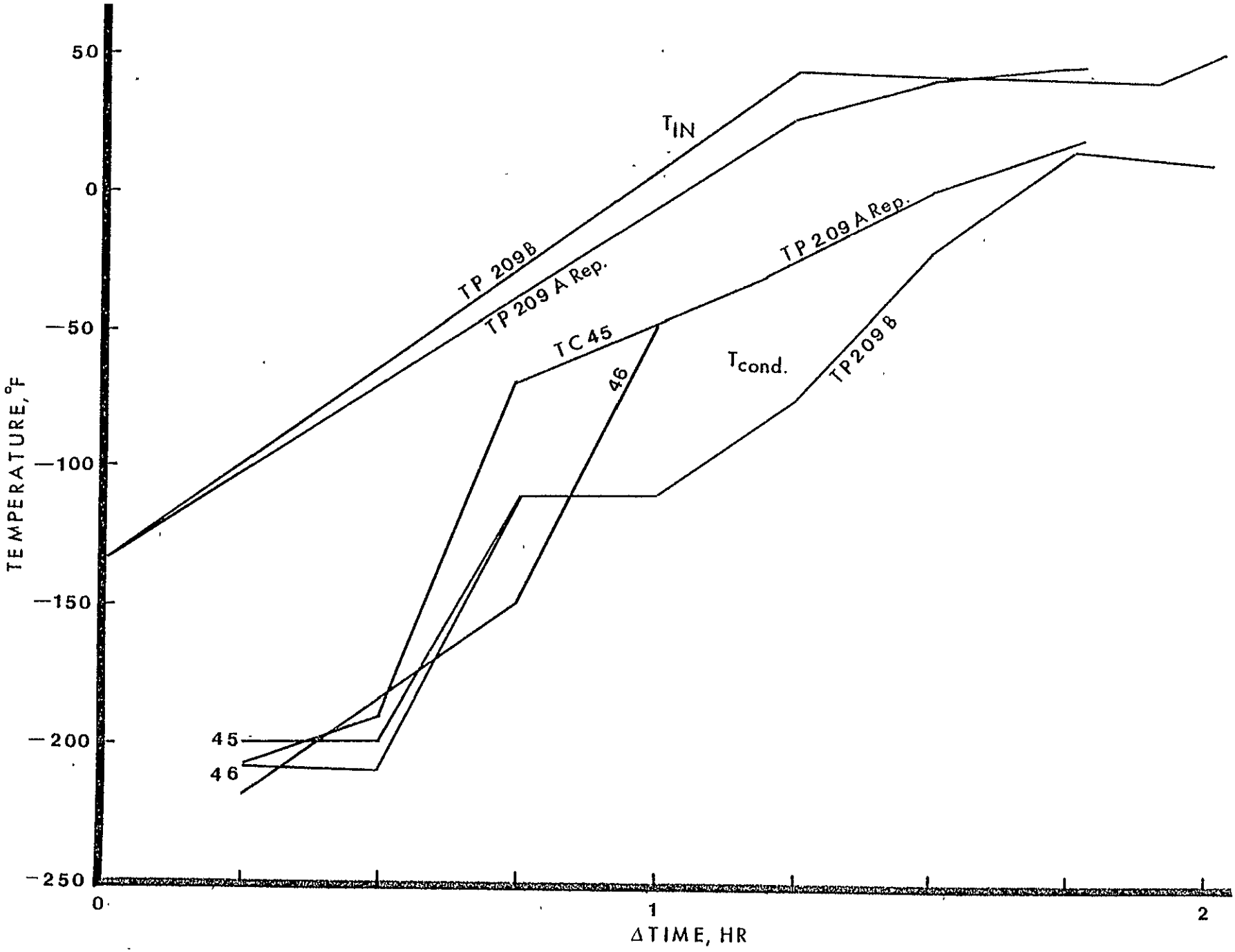

Figure 3.9 Comparison of T_{cond} for feeder No. 7 during thaws of Test Points 209B and 209A Rep.

their upward trend. Some delay for the phase change at the freezing point was expected.

It appeared that a heat-piping progression from the adiabatic section to the condenser was not initiated in feeder No. 11 and No. 12. as in the other feeder pipes during TP 209B, and as took place in all feeders during TP 209A Rep. No explanation can be given.

3.3 Value of the propane heat pipe

If the propane pipe had a significant heating effect then the thaw recovery time of feeder No. 2, which was the ammonia heat pipe contiguous to the propane heat pipe, should have been considerably less than feeder No. 12, but as the data show, Figs. 3.4 and 3.5, it was not. Thus, it is concluded that the major heat-transfer sources for the freeze-thaw recovery came from inside the heat pipes and axial conduction through the walls of the feeder tubes rather than from transverse heat conduction through the panel fins initiated by the propane heat pipe.

4.0 RECOMMENDATIONS

1. Experimentally verify the multipanel performance of a heat-pipe radiator system consisting of several prototype panel modules.
2. A more thermally uniform simulator is necessary in order to provide closer comparisons between the computer model calculations and experimental results.
3. Each feeder heat pipe should have at least one thermocouple installed on the OD of the wall of the pipe near the mid-point of the panel. Then the ammonia thaw time can be determined more accurately than when determined by panel temperatures.
4. The possibility of reducing the ΔT ($\simeq 25^\circ$ F, Q = 7900 BTU/HR from the feeder heat pipe to the panel by fabrication changes should be studied.
5. The twice-observed degradation of performance at maximum panel capacity needs further clarification.
6. Tests should be made with and without the propane feeder heat pipe to establish experimentally its aid in reducing thaw times.
7. Minimum panel conditions for a successful thaw should be determined.
8. Criteria for freezing, steady-state freeze performance and thawing should be derived.

5.0 CONCLUSIONS

1. The performance of the prototype panel was close to predicted in spite of a non-uniform environment.
2. The experimental data indicated that the propane heat pipe contributed little to a rapid thaw of the panel and was probably not needed.
3. Although the prototype panel had a 11 in heat-pipe spacing compared to a 8 in spacing for the feasibility panel, both panels gave similar values of Q_{REJ}/A. The prototype panel performance was improved significantly by immersing the feeder heat pipe evaporators into the coolant flow, which reduced the ΔT between coolant and ammonia vapor from a relatively high to a negligible value. The more significant Q_{REJ}/W values favored the prototype panel by about 21 percent.
4. Unlike the feasibility panel data, the measured fin-temperature distributions agreed reasonably well with theoretical predictions, the nonuniform simulator notwithstanding.
5. Freezing and thawing of the ammonia feeder heat pipes had no deleterious effect on their effectiveness.
6. With $\dot{m} \approx 597$ LB/HR and $Q_A \approx 8.0$ BTU/HR-FT^2, the feeder heat pipes were thawed and heat piping in 71 min while the freon temperature was increasing from -150° F to -25° F.
7. At maximum heat-transport conditions, a wide variation in individual feeder heat-pipe performance was observed.

6.0 REFERENCES

1. Sellers, J. P., Jr., "Steady State operation of a Heat-Pipe Radiator System: Analytical and Experimental", JSC-EC-R-74-1, L. B. Johnson Space Center, December 1973.

2. Sellers, J. P., Jr., "Steady State and Transient Operation of a Heat-Pipe Radiator System", HP-1, Tuskegee Institute, December 1974.

3. Sellers, J. P., Jr., "Third Annual Report: Heat Pipe Radiators for Space", HP-2, Tuskegee Institute, January 1976.

4. Swerdling, B. and Alario, J., "Heat Pipe Radiator: Final Report", HP4-14, Grumman Aerospace Corporation, October 1973.

5. Tawil, M., Alario, J., Prager, R., and Bullock, R. "Heat Pipe Applications for the Space Shuttle," AIAA Paper No. 72-272.

6. Turner, R. C., "The Constant Temperature Heat Pipe - A Unique Device for the Thermal Control of Spacecraft Components". AIAA Paper No. 69-632.

7. Deverall, J. E., Salmi, E. W., and Knapp, R. J., "Heat Pipe Performance in Zero Gravity Field," Spacecraft and Rockets, AIAA, Vol. 4, No. 11, 1967, pp. 1556-1557.

8. Harwell, W., Edelstein, F., McIntosh, R., and Ollendorf, S., "Orbiting Astronomical Observatory Heat Pipe Flight Performance Data", AIAA 8th Thermophysics Conference.

9. McIntosh, R., Knowles, G., and Hemback, R. J., "Sounding Rocket Heat Pipe Experiment", AIAA Paper No. 72-259.

10. Marcus, B. D., "Theory and Design of Variable Conductanct Heat Pipes", NASA CR-2018, April, 1972.

7.0 SYMBOLS

A	Surface area, FT^2
c_p	Specific heat of the coolant, BTU/LB-°F
L_{chp}	Length of the condenser portion of feeder heat pipes, FT
$\dot{m}$	Flow rate of the coolant, LB/HR
Q_A	Absorbed heat flux, $BTU/HR-FT^2$
Q_{REJ}	Total heat rejected by the panel, BTU/HR
T_{ad}	Adiabatic section temperature, °F
T_R, T_{nR}	Panel fin root temperature, °F
T_{IN}	Temperature of the coolant as it enters the header, °F
T_{cond}	Outside wall temperature of feeder condenser, °F
T_{FR}	Mean temperature of coolant, °F
T_p, T_P, T_{panel}	Panel fin temperature, °F
T_V	Temperature of the vapor in the feeder heat pipe ($\simeq T_{ad}$), °F
VCHP	Variable Conductance heat pipe
W	Weight of panel and header, LB
σ	Stephen-Boltzman constant $\doteq .1714 \times 10^{-8}$ $BTU/HR-FT^2-°R^4$
ΔT	Coolant temperature drop across the header, °F